Biomaterials 80 (2016) 80–95

Contents lists available at ScienceDirect

Biomaterials

journal homepage: www.elsevier.com/locate/biomaterials

The effect of silver or gallium doped titanium against the multidrug resistant *Acinetobacter baumannii*

A. Cochis [a, b], B. Azzimonti [a, c, 1], C. Della Valle [d, 1], E. De Giglio [e, 1], N. Bloise [f], L. Visai [f, g], S. Cometa [h], L. Rimondini [a, c, *], R. Chiesa [d]

[a] Department of Health Sciences, Medical School, University of Piemonte Orientale (UPO), Via Solaroli 17, 28100 Novara, Italy
[b] Department of Biomedical, Surgical and Dental Sciences, Università di Milano, via Beldiletto 1, 20142 Milan, Italy
[c] Consorzio Interuniversitario Nazionale per la Scienza e Tecnologia dei Materiali (INSTM), Via Giusti 9, Local Unit Piemonte Orientale, 50121 Firenze, Italy
[d] Department of Chemistry, Materials and Chemical Engineering 'G.Natta', Politecnico di Milano, Via Mancinelli 7, 20131 Milano, Italy
[e] Department of Chemistry, University of Bari "Aldo Moro", Via E. Orabona 4, 70126 Bari, Italy
[f] Molecular Medicine Department, Center for Health Technologies (CHT), UdR INSTM, University of Pavia, Viale Taramelli 3/b, 27100 Pavia, Italy
[g] Department of Occupational Medicine, Toxicology and Environmental Risks, S. Maugeri Foundation, IRCCS, Via S. Boezio 28, 27100 Pavia, Italy
[h] Jaber Innovation s.r.l., Via Calcutta 8, 00100 Roma, Italy

ARTICLE INFO

Article history:
Received 17 June 2015
Received in revised form
12 November 2015
Accepted 29 November 2015
Available online 2 December 2015

Keywords:
Acinetobacter baumannii
Biofilm
Gallium
Silver
Titanium
Anodic spark deposition

ABSTRACT

Implant-related infection of biomaterials is one of the main causes of arthroplasty and osteosynthesis failure. Bacteria, such as the rapidly-emerging Multi Drug Resistant (MDR) pathogen *Acinetobacter Baumannii*, initiate the infection by adhering to biomaterials and forming a biofilm. Since the implant surface plays a crucial role in early bacterial adhesion phases, titanium was electrochemically modified by an Anodic Spark Deposition (ASD) treatment, developed previously and thought to provide osseo-integrative properties. In this study, the treatment was modified to insert gallium or silver onto the titanium surface, to provide antibacterial properties.

The material was characterized morphologically, chemically, and mechanically; biological properties were investigated by direct cytocompatibility assay, Alkaline Phosphatase (ALP) activity, Scanning Electron Microscopy (SEM), and Immunofluorescent (IF) analysis; antibacterial activity was determined by counting Colony Forming Units, and viability assay.

The various ASD-treated surfaces showed similar morphology, micrometric pore size, and uniform pore distribution. Of the treatments studied, gallium-doped specimens showed the best ALP synthesis and antibacterial properties.

This study demonstrates the possibility of successfully doping the surface of titanium with gallium or silver, using the ASD technique; this approach can provide antibacterial properties and maintain high osseo-integrative potential.

1. Introduction

The increasing clinical use of implanted orthopedic medical devices, owing partly to the aging population, has lead both to the emergence of new diseases and to rising public-health costs. Infections related to biomaterial implantation are a major clinical problem, bringing high rates of morbidity and mortality [1], mainly owing to the formation of biofilm, which is recalcitrant to antimicrobial agents. The World Health Organization (WHO) has recently recognized antimicrobial resistance as one of the three most important problems affecting human health [2]. Multi Drug Resistant (MDR) pathogens have been identified with the acronym

Abbreviations list: ASD, Anodic Spark Deposition; AgCis material, Antibacterial agent ($AgNO_3$) with chelating agent (L-Cysteine); AgNPs material, Silver Nano-Particles; GaCis, Antibacterial agent ($Ga(NO_3)_3$) with chelating agent (L-Cysteine); GaOss, Antibacterial agent ($Ga(NO_3)_3$) with chelating agent (oxalic acid); ESKAPE, *Enterococcus faecium*, *Staphylococcus aureus*, *Klebsiella pneumoniae*, *Acinetobacter baumannii*, *Pseudomonas aeruginosa*, and *Enterobacter* spp; MDR, Multi Drug Resistant.

* Corresponding author. University of Piemonte Orientale (UPO), Department of Health Sciences, Via Solaroli 17, 28100 Novara, Italy.

E-mail addresses: andrea.cochis@med.uniupo.it (A. Cochis), barbara.azzimonti@med.uniupo.it (B. Azzimonti), cinzia.dellavalle@gmail.com (C. Della Valle), elvira.degiglio@uniba.it (E. De Giglio), nora.bloise@unipv.it (N. Bloise), livia.visai@unipv.it, livia.visai@fsm.it (L. Visai), stefania.cometa@virgilio.it (S. Cometa), lia.rimondini@med.uniupo.it (L. Rimondini), roberto.chiesa@polimi.it (R. Chiesa).

[1] These authors equally contributed to the work.

http://dx.doi.org/10.1016/j.biomaterials.2015.11.042
0142-9612/

"ESKAPE," standing for *Enterococcus faecium, Staphylococcus aureus, Klebsiella pneumoniae, Acinetobacter baumannii, Pseudomonas aeruginosa, and Enterobacter spp*. Of these, *A. Baumannii* is now the most dangerous strain in hospital-acquired infections [3], since it specifically targets moist tissues exposed by surgical procedures, adheres to implanted surfaces, forms biofilm [4] and, if untreated, leads to septicemia and death [5]. Its multidrug resistance [6] is caused by resistance gene "islands" which, under antibacterial pressure, can be rapidly switched. Sequence similarity and phylogenetic analyses have confirmed that most of these islands have been acquired from bacteria of unrelated genera, such as *Pseudomonas, Salmonella* or *Escherichia* [7].

It is thus a clinical imperative to prevent bacterial colonization and subsequent biofilm adhesion. Since the surface of implanted biomaterials plays a crucial role in early bacterial adhesion phases, a number of natural and synthetic materials have already been investigated: titanium and titanium alloys have been demonstrated to be biocompatible and to have appropriate mechanical properties [7,8]. Further, several inorganic antimicrobial agents have also been studied for their efficacy in the management of infections, including silver and gallium [9,10]. The antibacterial properties of silver have been extensively studied; more recently. it has also been shown that gallium has antibacterial properties, since it replaces Fe^{3+} in bacterial metabolism. Its anti-resorptive effects on bone and bone fragments show that it is adsorbed onto the surface of bone, where it is effective in blocking osteoclast resorption, without appearing to be cytotoxic to osteoclasts, nor to inhibit cellular metabolism.

Alongside its direct action on osteoclasts, gallium can also stimulate bone formation by acting on osteoblasts; a gallium nitrate formulation ($Ga(NO_3)_3$) is already in clinical use, and large doses are given to treat hypercalcemia or malignancy [11].

Based on these premises, in the present study biomimetic antibacterial silver and gallium surface modification treatments were developed for titanium implants. In particular, the morphological, physico-chemical, biological, and antibacterial characterization of silver- and gallium-modified titanium surfaces are reported, in order to investigate their anti-bacterial effectiveness against the emergent MDR *A. baumannii*.

2. Materials and methods

2.1. Morphological and chemico-physical characterization

2.1.1. Preparation of titanium specimens

Pure grade 2 titanium disks (medical grade ISO 5832-2, diameter: 12 mm; thickness: 0.5 mm) were cleaned by ultrasonic rinsing (Elma Elmasonic S 60/H, Germany) in acetone for 10 min and rinsed in Millipore water for a further 10 min. The disks were then dried in a thermostatic oven at 37 °C for 2 h.

2.1.2. Biomimetic treatment by Anodic Spark Deposition (ASD)

The titanium surface was modified by biomimetic treatment, capable to improve the osteointegration of titanium implants, using the Anodic Spark Deposition (ASD) technique, as described elsewhere [12], with a programmable DC power supply (N5772A, Agilent Technologies, Everett, WA, USA). Briefly, the titanium disks were connected as anode to the DC power supply system, while a commercially-pure grade 2 titanium net was used as cathode. Electrochemical treatment was performed under stirring and controlled temperature ($T = 0 \pm 1$ °C) with disks submerged in the electrochemical solution. At the end of the ASD treatment, the disks were subjected to chemical alkali treatment, immersing them in 5 M NaOH for 2 h at 60 ± 2 °C, in order to increase the surface calcium/phosphorous (Ca/P) ratio, as described elsewhere [13]. The resulting material was identified by the abbreviation SiB.

2.1.3. Gallium and silver doped titanium

Different antibacterial surface modifications were achieved by adding antibacterial species (gallium or silver) to the electrochemical solution used to treat the SiB disks [14]; cysteine and oxalic acid were added to the electrochemical solution as chelating compounds, to avoid precipitation of Ga salts during the electrochemical treatment, and to enhance Ga ion migration toward the anode. No final alkali treatment was applied to these materials. SiB disks free of antibacterial elements were used as controls, versus test disks modified with silver nanoparticles (AgNPs material), silver ions (AgCis material), or gallium ions (GaCis and GaOss materials); cysteine or oxalic acid, respectively, were added (Table 1).

2.1.4. Morphological characterization

Scanning electron microscopy (SEM) was used to investigate the resulting coatings. Briefly, specimens were sputter-coated with gold and analyzed with SEM (Zeiss-Evo 50 EP, Zeiss, Germany). Profilometric analysis was also carried out, using a laser profilometer (LP) (UBM-Microfocus Compact, NanoFocus AG, Germany). Three 3 × 3 mm^2 areas of each specimen were examined, with point density of 500/mm; the parameters Ra, Rt, and K were considered for roughness analysis. The thickness of the modified oxide film on cross-sections of the anodized specimens was investigated by metallographic analysis. Cross-sections were prepared by cutting the specimens, which had been embedded overnight in epoxy resin (Mecaprex, PRESI, Grenoble, France), abraded with paper (mesh 120, 320, 600, then 1200), and polished with diamond (6 μm diamond powder) and alumina paste (0.1 μm alumina powder). Optical microscopy (Leica DMLM, Switzerland) observations were at 500× magnification, and the thickness of the titanium oxide layer was calculated as the mean of measurements made on three cross-sections for each treatment (Software Leica LAS – Camera Leica DFC 290). Five cross-sections per disk were analyzed.

2.1.5. Chemical analysis by EDS

The chemical composition of each coating was qualitatively investigated by Elemental Dispersive X-Ray Spectroscopy (EDS); specimens were prepared as described above for SEM analysis, and analyzed with a Stereoscan 360 (Cambridge, UK). The EDS analysis was carried out on 500× acquired images (Oxford, Inca energy 200) that corresponded to surface portions of approximately 170 μm × 230 μm. X-Ray Diffraction (XRD) was used to analyze the structure of the materials. The X-Ray diffractometer (Philips PW 1710) was set at V = 40 kV and A = 40 mA. The angular range investigated was 0–70°, with a scanning speed of 2°/min. Analyses were run at a source wavelength of 1.54056 Å using a Ni-filter Cu Kα1 radiation, on the titanium disks modified by the ASD treatments.

2.1.6. X-ray photoelectron spectroscopy

X-ray photoelectron spectroscopy (XPS) was done using a Thermo VG Thetaprobe spectrometer (Thermo Fisher Scientific, Inc., Waltham, MA, USA), equipped with a microspot monochromatized AlKα source. The AlKα line (1486.6 eV) was used throughout the analyses, and the base pressure of the instrument was 10^{-9} mbar. The X-ray beam spot was 300 μm. Survey scans (binding energy (BE) range 0–1200 eV, FAT mode, pass energy = 150 eV) and detailed spectra relevant to Ti2p, C1s, O1s, Ca2p, P2p, Na1s, Si2p and Ag3d or Ga2p (FAT mode, pass energy = 50 eV) were recorded. Data analysis was performed using the Avantage software package (version 4.75, 1999–2010 Thermo Fisher Scientific©), which is a non-linear least squares fitting

Table 1
Experimental matrix of the selected treatments (*SiB–Na represents the control treatment; ^AT represents the alkali etching treatment performed according to par. 3.1.2.2).

Treatment	Antibacterial agent	Antibacterial conc.	Additive	Additive [M]	Current [mA/cm2]	Potential [V]	Time treatment [min]
SiB–Na*	–	–	–	–	10	295	13 m ± 2 m ^AT: 120 m
AgCis	$AgNO_3$	0.004 M	L-cysteine	0.002 M	10	295	12 m ± 30s
GaCis	$Ga(NO_3)_3$	0.004 M	L-cysteine	0.006 M	10	295	12 m ± 15s
GaOss	$Ga(NO_3)_3$	0.004 M	Oxalic Acid	0.306 M	10	325	10 m ± 1 m
AgNPs	Silver Nanoparticles (50 nm)	3 g/L	–	–	10	295	11 m ± 1 m

program. The maximum error on each peak position was ±0.2 eV. Charge referencing of all the experimental BE values was achieved by setting the C1s electrons of hydrocarbon contaminants on the specimen surface (from an adventitious carbon) at 285.0 eV. Gallium and titanium signals, arising from 2p orbitals, as well as the silver signal, arising from the 3d orbital, consisted of doublets relevant to the $2p_{3/2}$ and $2p_{1/2}$ or $3d_{5/2}$ and $3d_{3/2}$ components. The doublets showed a characteristic distance, i.e. 6.0 eV, 6.17 eV and 5.54 eV for Ag3d, Ga2p and Ti2p peaks, respectively [15]. Quantification (atomic percentage, At %) was by peak area.

Data from different elements were made comparable by correction with empirically-derived atomic sensitivity factors [16]. All atomic percentages are reported as means ± standard deviation, and data were averaged over at least four points per specimen analyzed.

2.1.7. Contact angle measurements

The static contact angle (SCA) was measured to investigate surface wettability. Three drops (2 μL/drop) of ultrapure distilled water (MilliPore) were expelled from a micrometric syringe and deposited on each specimen surface analyzed; three specimens per material were tested. The wettability studies were performed with a contact angle video based system (Contact Angle System OCA15 plus, Dataphysics, Germany) and analyzed with the SCA20 software (Dataphysics, Germany).

2.1.8. Mechanical properties

Indentation tests were run to determine the elastic modulus (E) and hardness (H) of the ASD film [17]. The indentations were made with a micro-indenter (Fischerscope H100, Germany) following ISO 14577-1 standard, analyzing cross-sections of the disks through the oxide surface layer, as reported above. The incremental load applied varied logarithmically from 0 to 10 mN, and the load was applied using a diamond Vickers tip. A load vs. displacement curve was recorded, and the E and H were calculated. The indenter depth was maintained at below 10% of the measured film thickness, to avoid substrate effect on H and E.

To analyze the susceptibility of the coating to delamination, a three-point bending test was performed: the treated specimens were placed on a support span with two rollers, and a single upper roller with a 5 mm section applied the load. Rollers were mounted on the electromechanical INSTRON machine (mod. 8062, Norwood, MA, USA) operating in the position control method. The distance between rollers was 40 mm. A force was then applied with a slow speed (10 mm/min) until a flexion of 30° was attained.

The scratch test was used to evaluate the adhesion of the modified oxide coating to the underlying substrate. The scratch test was conducted using a MCTX S/N: 50-00223 (CSM Instruments, Switzerland) scratch tester with a linear and progressive load, with the following test parameters: scratch pre-load of 0.03 N, load speed of 5 N/s, maximum load 30 N. The scratch length was 3 mm. The scratch test consisted of generating scratches using a Rockwell C diamond tip with 200 μm radius (serial number V-264) maintained at a constant speed over the surface under different test loadings. The critical load was here defined as the smallest load at which a recognizable adhesive failure to the underlying substrate occurred. Using the critical load, the corresponding shear stress τ_c was calculated using the model expression developed by Ollivier and Matthews [18].

2.1.9. Antibacterial element release evaluation

Inductively Coupled Plasma - Optical Emission Spectrometry (ICP-OES, Perkin Elmer Optima 2000DV OES, Wellesley, USA) analysis was used to investigate the release of antibacterial agents. To determine release of Ag and Ga from the surface, 15 specimens for each treatment were incubated in 5 ml of calcium-free D-PBS (Dulbecco's modified Phosphate buffer solution, Sigma, Saint Louis, MO, USA). They were fixed vertically in 15 mL falcon tubes with conical end, to allow release of the antibacterial agents from both sides of the specimen. The tubes were maintained at 37 °C in a thermostatic oven under constant gentle shaking (50 rpm) (VDRL DIGITAL MOD. 711/D). After 1, 4, 7, 14 and 21 days, the pooled solution from three specimens per treatment was analyzed by ICP-OES, to determine the concentration of the elements released. The D-PBS solution was also analyzed by ICP-EOS to standardize the data.

2.2. Biological characterization

2.2.1. Eukaryotic cell cultures and growth conditions

The human primary osteogenic sarcoma Saos-2 cell line (ECACC 89050205, European Collection of Cell Cultures, distributed by Sigma–Aldrich, Milan, Italy) was cultured in McCoy's 5A medium (Gibco, distributed by Life technologies, Milan, Italy) supplemented with 10% heat-inactivated Fetal Bovine Serum (FBS, Sigma–Aldrich), 1% sodium pyruvate, penicillin, streptomycin, and gentamycin (all from Sigma–Aldrich) in an incubator at 37 °C with a 5% CO_2 atmosphere. When 80–90% confluent, cells were detached with a trypsin/EDTA solution (GIBCO Invitrogen, Milan, Italy), counted using a hemochromocytometric grid (Neubauer chamber), and plated at the proper density.

2.2.2. Direct cytocompatibility evaluation

Cells in direct contact with the modified surfaces were evaluated. Treated disks (six/treatment) were placed in 24-well tissue culture plates, and 1×10^4 Saos-2/cm^2 were seeded onto the disks in 500 μL of complete McCoy's 5A medium. After 24 h the disks were transferred into new sterile 24-well plates containing 500 μL of fresh medium for 1, 4, 7, 14 and 21 days. At each time point, culture medium was replaced with 100 μL of 10% Alamar Blue solution and cell viability was measured as described above. After rinsing with 37 °C PBS and flooding with 500 μL fresh culture medium, plates were replaced in the incubator. The medium was changed every 24 h until completion of the assay.

2.2.3. Saos-2 alkaline phosphatase activity

To test osteogenic activity, four samples of cells from 4, 7 and 21 day time-point treatments were removed and washed three

times in 500 μL of 37 °C PBS, dried and examined for Alkaline Phosphatase (ALP) activity. ALP activity was determined colorimetrically with the Alkaline Phosphatase Assay Kit (Abcam, Euroclone, Pero, Milan, Italy) and standardized on the total protein concentration calculated with the Thermo Scientific BCA Protein assay reagent (Pierce, distributed by Thermo Fisher Scientific, Italy).

2.2.4. Saos-2 morphology investigation by SEM and immunofluorescence

One day after culturing the Saos-2 cells on the surface of the disks, the cell morphology was examined by SEM. Briefly, after supernatant removal, cell samples were gently washed with sterile PBS1x and fixed in 2.5% glutaraldehyde in 0.1 M sodium-cacodylate buffer at pH 7.4 for about 2 h. After fixation, the cells were gently washed three times with 1 mL of sodium-cacodylate buffer. They were then dehydrated in ethanol (25, 50, 75, 96, and 100%), freeze-dried overnight, mounted on SEM stabs, sputter-coated with gold, and analyzed by SEM (ZEISS-EVO 50 EP, Italy).

Immunofluorescent morphological staining was also assessed. 10,000 cells were seeded onto each disk and incubated for 24 h at 37 °C in complete medium. After 4% paraformaldehyde fixation, cells were permeabilized with 0.1% Triton x-100 at 4 °C for 30 min, and stained with mouse anti-α-Tubulin-Alexa 488 (2 μg/mL, EX/EM maxima 495/519 nm, Invitrogen, Life technologies, San Giuliano Milanese, Milan, Italy) for 45 min at RT. After rinsing, cells were stained with 50 μg/mL tetramethylrhodamine B isothiocyanate (TRITC) phalloidin conjugate solution (EX/EM maxima 540/575, Sigma–Aldrich, Milan, Italy) for 45 min at RT. They were mounted after counterstaining the nuclei with Hoechst 33342 (2 μg/mL, Sigma–Aldrich). The images were acquired with a digital image capture system (Olympus, Italy) at 20 and 40× magnifications.

2.3. Antibacterial activity evaluation

2.3.1. Prokaryotic cell cultures and growth conditions

One strain (DSM 30007), obtained from the Leibniz Institute DSMZ-German Collection of Microorganisms and Cell Cultures (Braunschweig, Germany), and two clinical isolates (named *AB1* and *AB2*) of the biofilm former *A. baumannii*, kindly provided by the Bacteriology and Virology Unit of "Azienda Ospedaliero-Universitaria Maggiore della Carità" (Novara, Italy), were grown for 24 h at 37 °C under aerobic conditions. The strains were cultivated on either Luria Bertani (LB; Difco, Ventura, CA, USA) or iron-chelated Minimal medium MM9 [19] agar plates, then harvested, diluted in PBS and standardized to 2×10^8 cells/mL using the Mc Farland standard 1.0 [20,21].

2.3.2. Antibacterial activity

One mL of the standardized cell suspensions was applied to the surface of 1 cm diameter disks placed in 24-well tissue culture plates (PBI International, Milan, Italy). The cells were left to adhere uniformly for 90 min at 37 °C at 120 rpm. Non-adherent cells were removed by gently washing with 1 ml of PBS. After adding fresh culture medium, controls and treated disks were incubated for 72 h at 37 °C at 120 rpm [22,23]. To allow the biofilm to detach from the disk surface, disks containing biofilms were re-suspended in 1 mL of PBS, vortexed and sonicated at 60 Hz (Aquasonic 250HT, VWR International) for 30 s; this was repeated five times. Aliquots of 100 μL suspension were transferred onto 96-well plates and used to prepare six tenfold dilutions, mixing 20 μL of biofilm suspension with 180 μL of saline. Twenty μL of each dilution were spotted onto agar plates and incubated for 24 h at 37 °C. The following day, the number of CFUs/disk was counted, working blind, and using the following formula: (number of colonies) × 10 × (reverse of dilution value) [24–26].

The colorimetric assay 2,3-bis (2-methoxy-4-nitro-

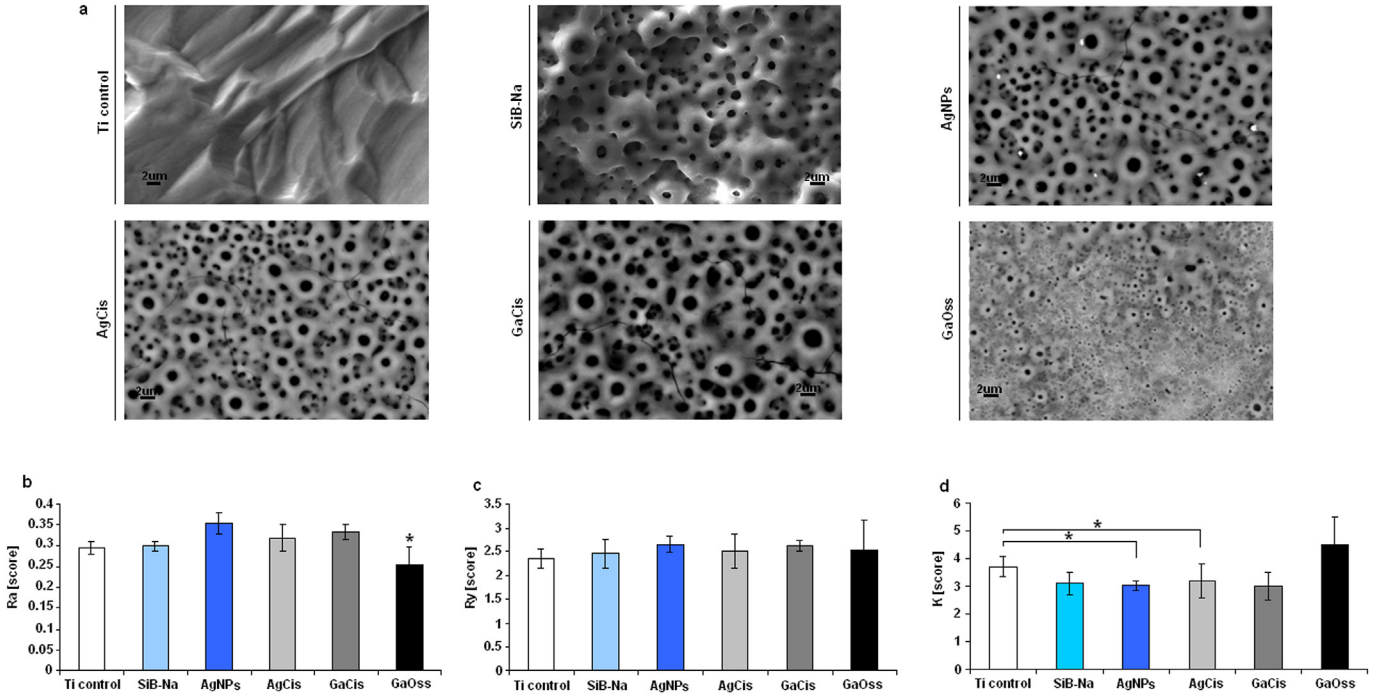

Fig. 1. a–d. Physical characterization of test surfaces. SEM morphology (a), average roughness (Ra) (b), maximum peak-to-valley height of the measurement area (Ry) (c) and kurtosis (K) (d). For the parameter Ra, the value for GaOss was significantly lower than all other treatments ($p < 0.05$, indicated by the asterisk), while for Ry there was no statistically significant difference between the test groups ($p > 0.05$). For the parameter K, GaCis and AgNPs were slightly lower than untreated titanium ($p < 0.05$, indicated by the asterisk). Data are presented as means and ± standard deviations; SEM images bar scale = 2 μm, magnification 150×.

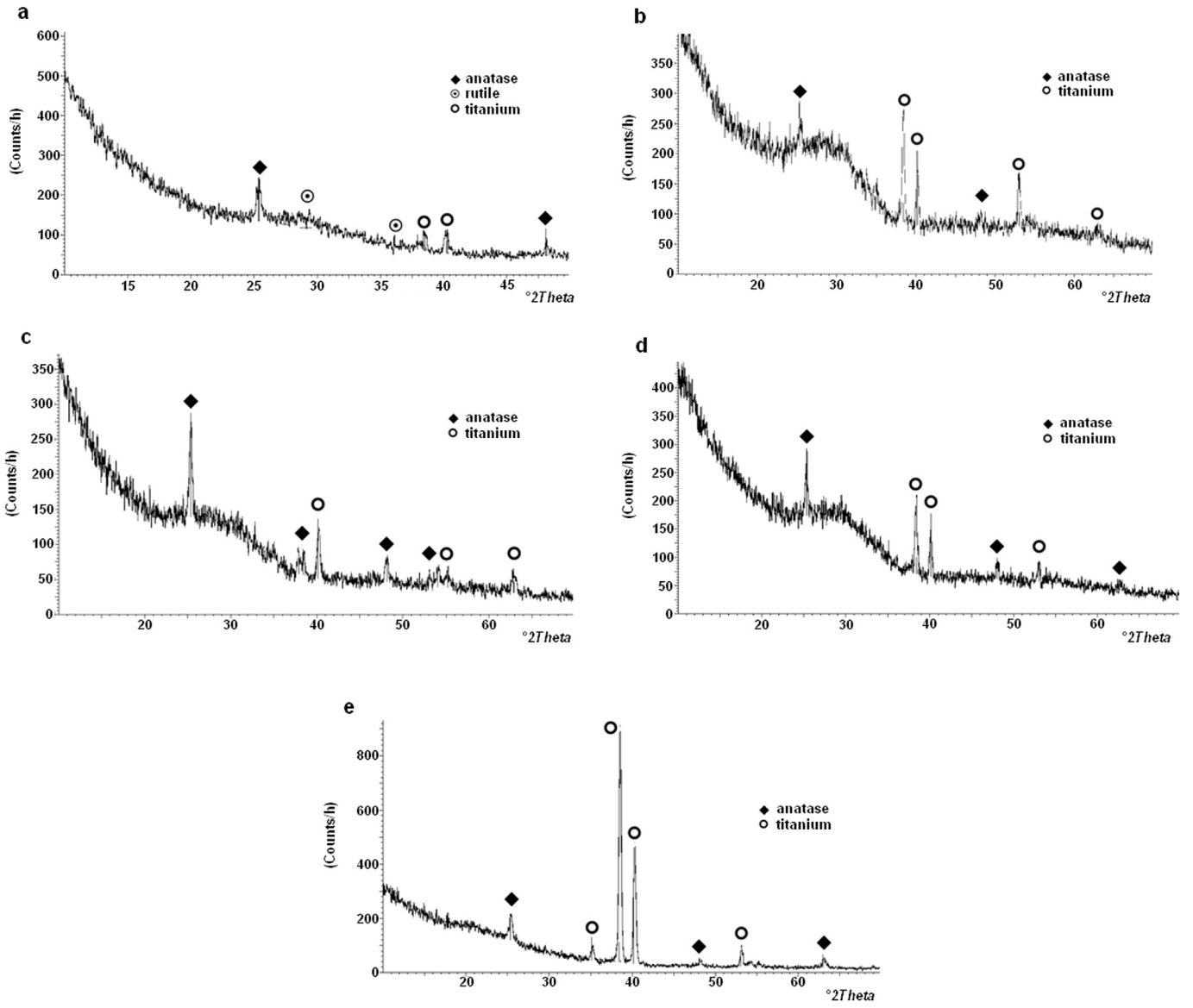

Fig. 2. a–e. XRD spectra of tested surfaces: SiB–Na control (a); AgNP (b); AgCis (c); GaCis (d); GaOss (e).

sulphophenyl)-5-[(phenyl amino) carbonyl]-2H-tetrazolium hydroxide (XTT, Sigma, St Louis, MO, USA) was used to determine the dehydrogenase activity, as an indicator of the metabolic state of the 72 h biofilm cells [27].

Seventy-two hours after culturing on the disk surface, *A. baumannii* morphology of each strain was analyzed by SEM, as described for the eukaryotic cell line.

2.4. Statistical data analysis

Statistical analysis was performed using Origin Pro Software. After having verified the normal distribution of variance, the one-way ANOVA test followed by Bonferroni's multiple comparison test were performed for the profilometric data analysis, while the biological data were analyzed using the one-way ANOVA test, followed by applying the independent two-sample two-way Student's t-test to the data for group comparison (significance level $p = 0.05$). The results are expressed as means ± standard deviation. Two-way ANOVA tests (different treatments and release times) were performed for the indirect cytotoxicity variance evaluation; after which the Student's t-test was applied to the data for group comparison.

3. Results

3.1. Morphological and chemico-physical characterization

3.1.1. SEM topographical characterization

Fig. 1a shows the SEM images of the different ASD treated surfaces and the controls. The figure shows the morphology of the titanium disk before any ASD treatment. The ASD-treated surfaces evidenced the microporous morphology typical of ASD treatments on titanium, characterized by micrometric pore size. Pore distribution appeared uniform for all ASD treatments, with pore dimension ranging from nanometers to 3 μm. In particular, when gallium nitrate was chelated with oxalic acid (GaOss), the pore diameter was smaller than with other ASD treatments. The morphology of GaOss might be the result of the fact that the voltage achieved was the highest of all the ASD treatments (325V, Table 1). Especially on AgNPs, both AgCis and GaCis treatments produced

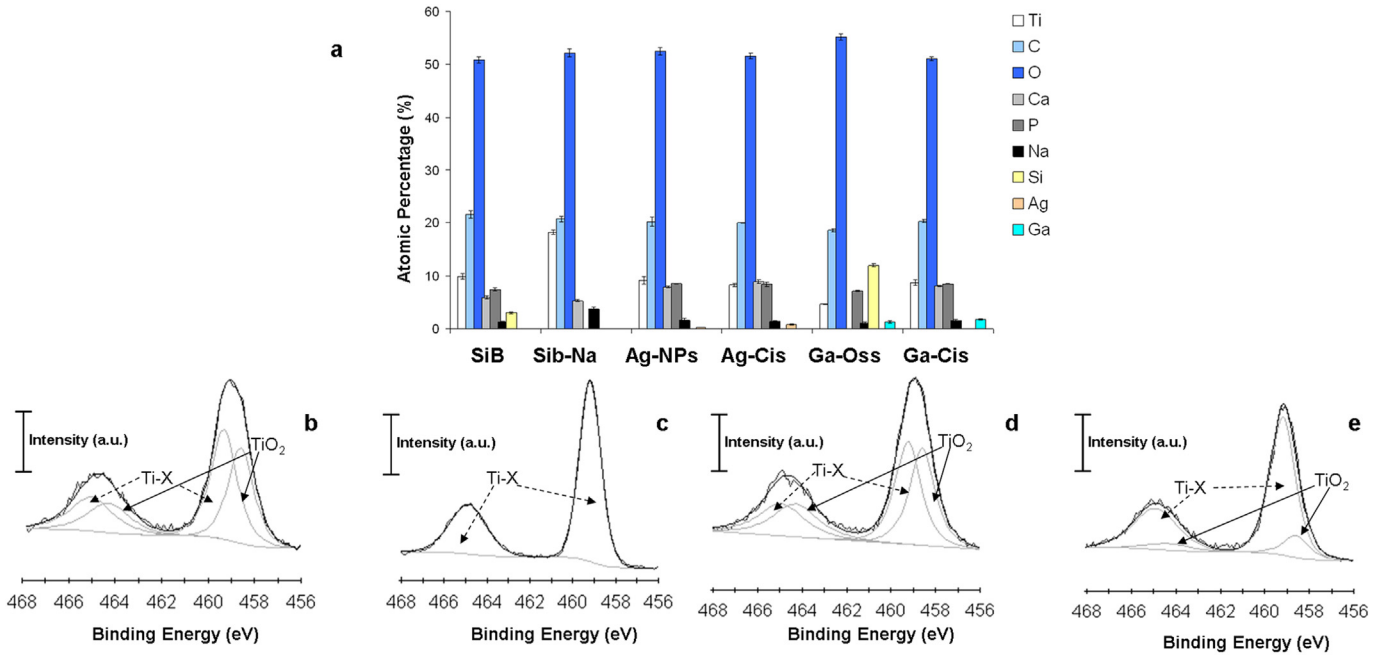

f

	SiB		SiB-Na		Ag-NPs		Ag-Cis		Ga-Oss		Ga-Cis	
	BE (eV)	At.%	BE (eV)	At %	BE (eV)	At %	BE (eV)	At.%	BE (eV)	At %	BE (eV)	At %
TiO_2	458.6	45.4	/	/	458.6	47.3	458.6	48.5	458.7	15.1	458.6	13.9
Ti-X	459.3	54.6	459.3	100	459.2	52.7	459.3	51.5	459.3	84.9	459.2	86.1

Fig. 3. a–f. XPS analysis. Surface chemical composition of SiB and SiB–Na treatments (controls) and of AgNPs, AgCis, GaOss and GaCis antibacterial treatments (a). Ti2p signals recorded on SiB (b), SiB–Na (c), silver-doped (d) and gallium-doped (e) specimens. Attributions, binding energies (BE) and atomic percentages (At %) relevant to the $Ti2p_{3/2}$ peaks of SiB, SiB–Na, silver-doped and gallium-doped samples (f).

some microcracks. No cracks were visible on control SiB–Na or GaOss. Silver nanoparticle aggregates were identifiable as white spots.

3.1.2. Surface roughness (LP)

Surface characteristics, among them average roughness (Ra, Fig. 1b), maximum peak-to-valley height of the entire measurement area (Ry, Fig. 1c) and kurtosis (K, Fig. 1d) parameter values, were evaluated for controls (Ti and SiB–Na) and ASD treatments. Ra was similar for all surfaces excluding GaOss (ANOVA: $p > 0.05$). Ra for GaOss was significantly lower than any other ASD treatment (ANOVA, all materials: $p < 0.05$). The Ry value was similar on all treated surfaces (one way ANOVA $p > 0.05$), being around 2.5 μm. The kurtosis coefficient was similar among all the surfaces studied, and above 3 in all cases, indicating that all surfaces are characterized by the presence of many peaks. In the case of GaCis and AgNPs, the K parameter was slightly lower than untreated titanium ($p < 0.05$), indicating a smoother surface profile.

3.1.3. Crystallographic structure of the ASD surfaces (TF-XRD)

The TF-XRD analysis for the different ASD treatments showed in all cases the presence of the crystallographic structure of titanium oxide (TiO_2) in the anatase form (main peak $2\theta = 25°$) in addition to titanium peaks (Fig. 2). The high anatase TiO_2 peaks for AgCis, AgNPs and GaCis treatments indicated the presence of a similarly thick titanium oxide layer on the surface. For GaOss, the titanium peaks were higher than the TiO_2 peaks, probably due to the thinner TiO_2 layer obtained with GaOss ASD treatment.

3.1.4. Element qualitative analysis (EDS)

The qualitative elemental composition obtained by EDS analysis (images not shown) highlighted the presence of calcium, phosphorous, and silicon on the SiB–Na control, as well as on all the ASD-modified specimens, with the exception of GaOss, on which the calcium signal was not detectable. Moreover, the SiB–Na control also showed the presence of sodium, ascribed to the post-treatment alkali etching after ASD. Ag was detectable by EDS analysis only in correspondence with a white spot visible on the SEM image, confirming the presence of silver nanoparticles within the AgNPs specimen, whereas Ag was not detected on the AgCis specimen. Conversely, EDS detected gallium both on GaCis and GaOss specimens; in particular the gallium peaks on GaOss were higher than those on GaCis.

3.1.5. XPS characterization

XPS was used to characterize the surface of specimens obtained by the proposed ASD treatments. The surface chemical composition of controls (SiB and SiB–Na) and antibacterial treatments (silver-based: AgNPs and AgCis; gallium-based: GaOss and GaCis), is given in terms of atomic percentages (Fig. 3a). Chemical etching with NaOH led to a surface sodium enrichment in the SiB–Na compared to the SiB specimens. This was revealed both by the Na/Ca signal area ratios (equal to 0.70 and 0.22 for SiB–Na and SiB specimens, respectively) and by the Na/Ti signal area ratios (0.20 and 0.13 for

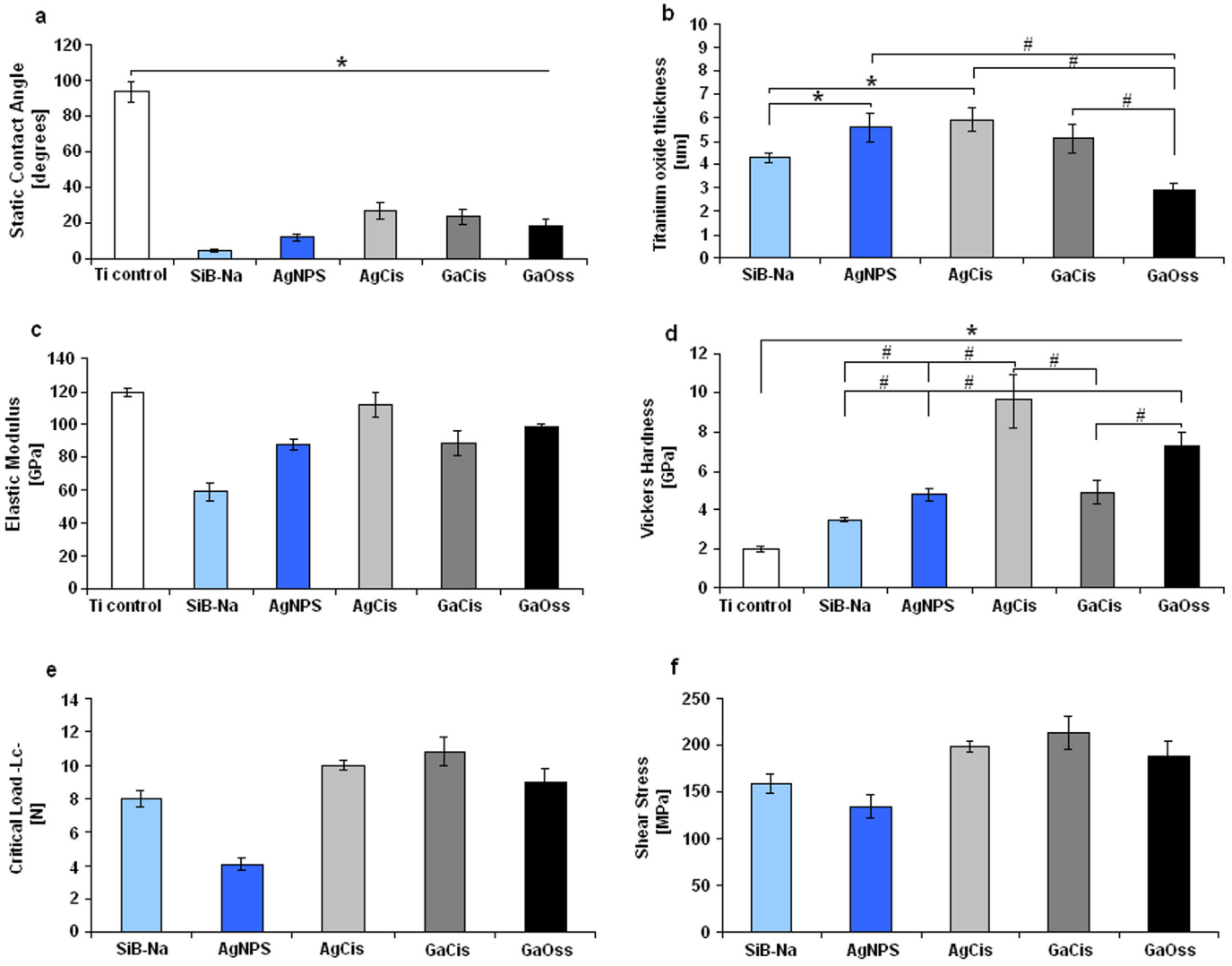

Fig. 4. a–f. Static contact angle measurement (a) showed that all ASD surfaces are more hydrophilic than untreated titanium ($p < 0.01$, indicated by the asterisk). Surface thickness measurements (b) of ASD modified titanium oxide layers revealed that AgCis and AgNPs are thicker than SiB–Na ($p < 0.05$, indicated by the asterisk), while GaOss was significantly thinner than other treatments ($p < 0.05$, indicated by #). Mechanical properties regarding elastic modulus (c) and Vickers hardness (d) showed that the ASD coatings were significantly harder than untreated titanium control ($p < 0.05$, indicated by *). Mechanical properties of critical load (e) and shear stress (f) did not differ significantly.

SiB–Na and SiB, respectively). The XPS data confirmed the presence of silver in both the silver-modified specimens. The signal area ratio Ag/Ti was equal to 0.02 for AgNPs and 0.10 for AgCis, evidencing a significantly larger amount of silver on the AgCis than on the AgNPs surface. As far as the gallium-modified specimens are concerned, XPS analysis detected gallium on both antibacterial specimens. The surface gallium amount calculated by evaluating the Ga/Ti signal area ratios was equal to 0.20 and 0.28, on GaCis and GaOss specimens, respectively. The BEs of $Ag3d_{5/2}$ on silver-based treatments were equal to 368.5 eV, while on both gallium-based treatments the $Ga2p_{3/2}$ signals showed an experimental BE equal to 1118.1 eV. Unlike GaOss surfaces, no silicon-containing species were detected on AgNPs, AgCis, or GaCis surfaces.

The presence of calcium and phosphorous on the treated surfaces is significant: the Ca/P signal area ratios were found to be 0.8, 0.93, 1.06 and 0.96, in SiB, AgNPs, AgCis and GaCis specimens, respectively. The binding energy of calcium (347.5 eV) and phosphorus (133.3 eV) in the specimens were in agreement with those of $Ca(H_2PO_4)_2$ and/or $CaHPO_4$ compounds.

As far as the Ti2p signals are concerned, the curve fittings of Ti2p for SiB, SiB–Na, and the silver- and gallium-containing specimens are in Fig. 3b–e; their contributions, together with their BE and At% values, are summarized in Fig. 3f. In particular, the Ti2p spectrum for SiB specimens showed two different contributions, i.e. one typical of TiO_2, and another (labeled Ti-X), ascribable to mixed titanates containing heteroatoms (Si, Ca, Na and P) with unknown stoichiometry (Fig. 3b). In the case of SiB–Na specimens, only Ti-X contributions were detected, thus excluding the presence of TiO_2 on the surface (Fig. 3c). Conversely, the Ti2p spectra for silver-containing specimens showed almost identical amounts of TiO_2 and Ti-X species (Fig. 3d), while in gallium-containing ones, Ti-X species made the main contribution, with only a little TiO_2 (Fig. 3e). Titanium signals recorded for AgNPs and AgCis, and for GaCis and GaOss specimens, did not differ significantly (Fig. 3f).

3.1.6. Contact angle measurement

Static contact angle measurements revealed that all the ASD surfaces possessed higher hydrophilicity than untreated titanium ($p < 0.01$) (Fig. 4a). In particular, the control surface SiB–Na had the greatest wettability, with an average static contact angle as low as

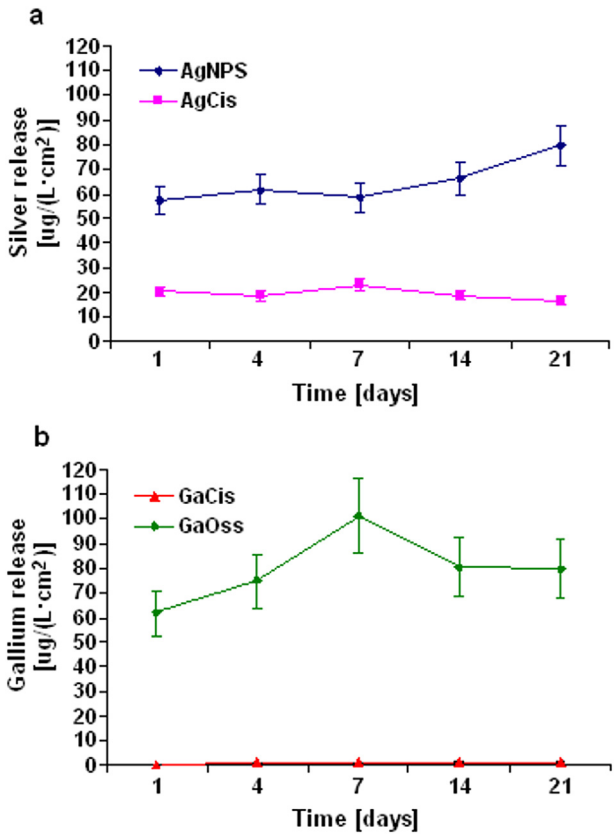

Fig. 5. a–b. Antibacterial agent release. Silver release (a) from AgCis occurred during the first 24 h, after which no further release was detected (release 23 μg/(Lcm^2), $p > 0.05$, indicated by *); silver release from AgNps was relatively constant over the first seven days, after which it increased up to 21 days (80 μg/(Lcm^2)). Gallium release from AgCis (b) was low and gradual from day 4–21 (release 1.3 μg/(Lcm^2)). Conversely, gallium was released from GaOss from day one (140 μg/(Lcm^2)) until day 7, after which no further release was observed.

5.0 ± 1.1. The AgNPs treatment showed the greatest wettability of all other treatments with Ag or Ga, while AgCis showed the lowest value (27.1 ± 4.7).

3.1.7. Titanium oxide thickness evaluation

The thickness of the ASD modified titanium oxide layers was evaluated by metallographic analysis on disk cross-sections (Fig. 4b). The thicknesses of AgCis, AgNPs, and GaOss were significantly different from the control SiB–Na ($p < 0.05$). In particular, AgCis and AgNPs had a greater thickness of titanium oxide, respectively being 5.9 ± 0.5 μm and 5.6 ± 0.6 μm. On the contrary, the GaOss treatment produced a significantly thinner layer than other treatments, at 2.9 ± 0.3 μm.

3.1.8. Elastic modulus and hardness

The elastic modulus and the hardness were measured by nano-indentation on the titanium oxide cross-sections, as used (above) to analyze the thickness of titanium oxide on the different ASD surfaces (Fig. 4c–d). In particular, the resulting Vickers hardness values were converted into the corresponding values indicated in GPa. Hardness of the ASD coatings was significantly higher than that measured on untreated titanium ($p < 0.05$). The AgCis and GaOss films showed the greatest hardness of all tested coatings ($p < 0.05$).

3.1.9. Three point bending test

The coating's susceptibility to delamination after tensile stress was evaluated by the three point bending test. SEM analysis was performed on the tensed parts of the surface ("stretched fibers" area). Although some cracks could be detected by SEM on SiB–Na, AgNps, GaCis and ACis (images not shown), no delamination was observed for any of the ASD treated surfaces.

3.1.10. Scratch test

Critical loads (Fig. 4e) and shear stress (Fig. 4f) values, obtained from the scratch test on the ASD surfaces, showed that the SiB–Na film was strongly adherent to the titanium substrate, and coating failure (critical load) occurred at 8 N. Moreover, no particulate was formed during film failure. The AgCis coating showed higher critical load (10.0 N) than the SiB–Na control, proving good film adhesion and high resistance to tip penetration. After reaching the critical load, the scratch track showed brittle fractures, with film cohesive failure and chip formation. The GaCis coating was very adherent (critical load 10.8 N), showing plastic deformation. At higher loads (≈16 N) the test only partially exposed the underlying substrate, indicating strong adherence of the film. The AgNPs film showed the weakest adhesion, with critical load at 4.1; at 7 N, the titanium surface was already considerably exposed. The GaOss film was strongly adherent to the substrate, with a critical load of 9.0 N, showing cohesive failure.

3.1.11. Release of antibacterial agents

The release of silver from AgCis, measured by ICP-EOS, occurred during the first 24 h, and was as low as 23 μg/(Lcm^2); no further release occurred after 24 h ($p > 0.05$) (Fig. 5a). The released silver was detected in 5 mL of D-PBS, with a maximum of 0.11 μg/cm^2. The silver release from AgNPs was initially constant until day 7, then slightly increased to 80 μg/(Lcm^2) until day 21, with total amounts released being 0.40 μg/cm^2.

GaCis showed a very low and gradual release of gallium (Fig. 5b) from the fourth day (1.1 μg/(Lcm^2)) after which it was stable until day 21 (1.3 μg/(Lcm^2)). GaOss showed much higher gallium release already after the first day (140 μg/(Lcm^2)), with values of 62 μg/cm^2. No additional release was observed from days 7–21.

3.2. Biological characterization

3.2.1. Saos-2 direct cytocompatibility assay

The metabolic activity of the cells in contact with the treated surfaces increased from days 1–21, as detected by the Alamar Blue assay (Fig. 6a); there was no statistically-significant difference in cell viability among the different surfaces at any time point ($p > 0.05$); no direct cytotoxic effect promoted by the antibacterial elements present on the surfaces was observed.

3.2.2. Alkaline phosphatase activity (ALP)

ALP synthesis incremented progressively from day 1 to day 21. In particular, at day 1, no significant difference was found between treated and untreated surfaces ($p > 0.05$). At day 7, the trend was still comparable ($p > 0.05$), though lower ALP synthesis ($p < 0.05$) was found in the untreated controls (Fig. 6b). At day 21, the ALP activity on the ASD surface was significantly higher compared to the titanium control ($p < 0.05$), confirming the data on osteoblast activity of the ASD coatings obtained at day 7. Interestingly, GaOss treatment showed significantly higher ALP activity than GaCis antibacterial treatment, and it was also higher than the SiB–Na control ($p < 0.05$). Thus the presence of gallium as antibacterial agent did not interfere with ALP production, probably determining a stimulating effect on osteoblast activity toward new bone-matrix formation.

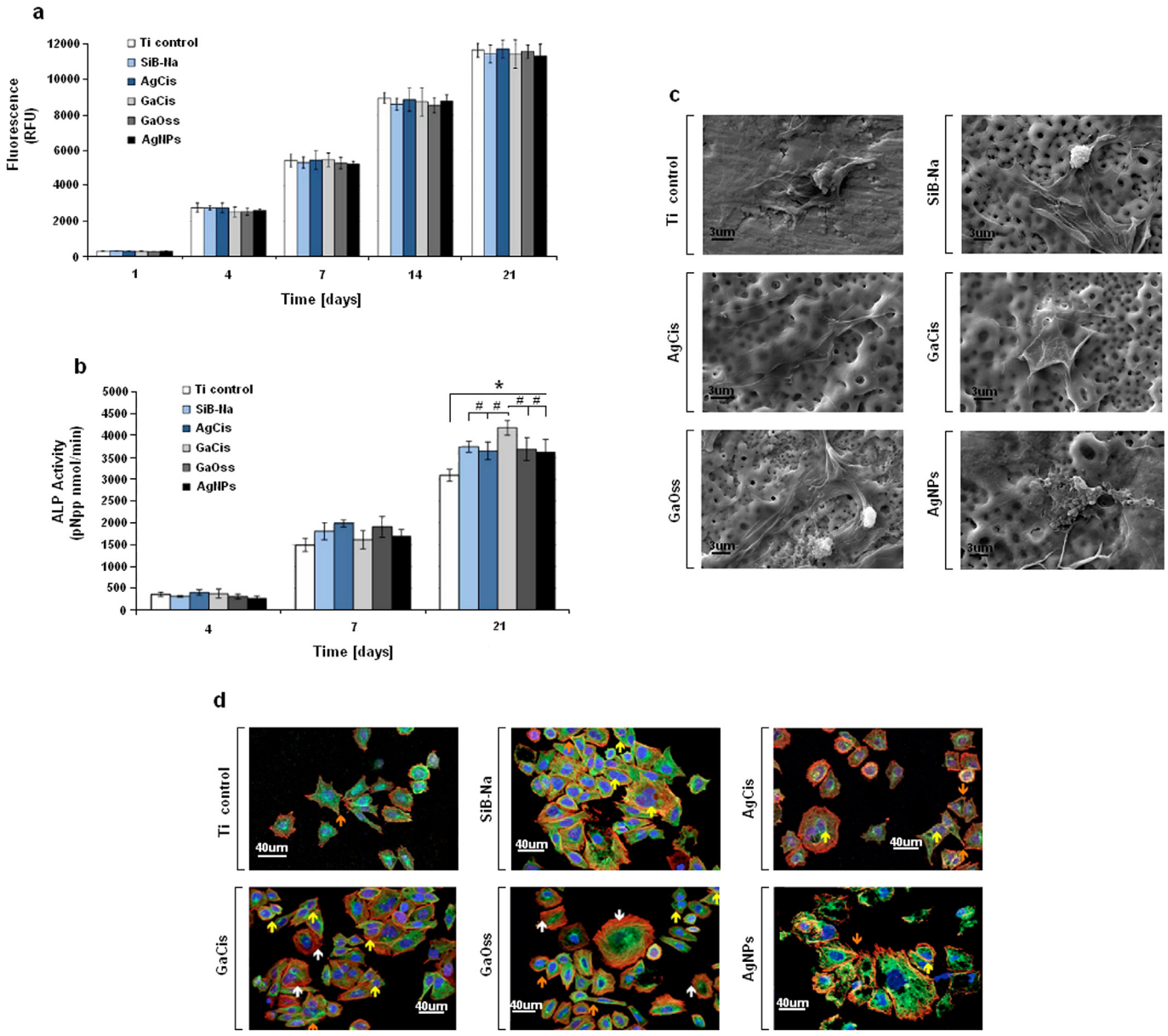

Fig. 6. a–d. *In vitro* cytocompatibility. Cell viability was comparable between control and treated specimens (a), whereas ALP activity (b) showed a statistically significant difference between control and treated groups ($p < 0.05$, indicated by #) and between GaCis and other groups ($p < 0.05$, indicated by *). SEM (c, bar scale = 3 μm; magnification = 1000×) and immunofluorescence staining (d, phalloidin, in red; α-tubulin in green, and dapi in blue; bar scale = 40 μm) morphological analysis showed no difference between cells cultivated on control and treated surfaces.

3.2.3. *SaOS-2 SEM adhesion study and immunofluorescence staining*

As shown by SEM analysis, after 24 h culture SaOS-2 cells that had attached onto the treated surfaces were completely flattened, with a branched shape and a morphology intimately following the porous structure of the modified titanium surfaces (Fig. 6c). Cells also adhered to the untreated surface, but the spreading was less consistent and less favorable. Regarding actin and α-tubulin cytoskeleton fluorescent labeling (Fig. 6d), osteoblast-like cells adhered to the treated surfaces, showing strong expression of both markers, and a replication phenotype (yellow arrows). Cell-to-cell interactions, and well-defined focal points (orange arrows) were also visible. Immunofluorescent analysis also confirmed SEM observation: the SaOS-2 cells spread to a lesser extent on untreated titanium, while on the GaCis and GaOss surfaces they were evident in the form of stress fibers [28] on actin filaments (white arrows).

3.3. *Antibacterial activity*

3.3.1. *Biofilm cells viability (XTT assay) and CFU count*

In general, after 72 h, all treated specimens differed significantly from untreated titanium controls ($p < 0.05$, Fig. 7a–b, indicated by *). Fig. 7 a–b gives the results obtained with *A. baumannii* strain DSM 30007 cultivated in LB medium; gallium-doped specimens performed best in terms of bacterial inhibition, and were significantly better than biomimetic SiB–Na and silver-doped specimens ($p < 0.05$, indicated by #). Both AgCis and AgNPs determined a reduction in bacterial viability of about 45 (±4) and 42 (±7) %, while gallium decreased viability by 71 (±9) and 53 (±3) % for GaCis and GaOss respectively (Fig. 7a). Moreover, GaCis differed significantly

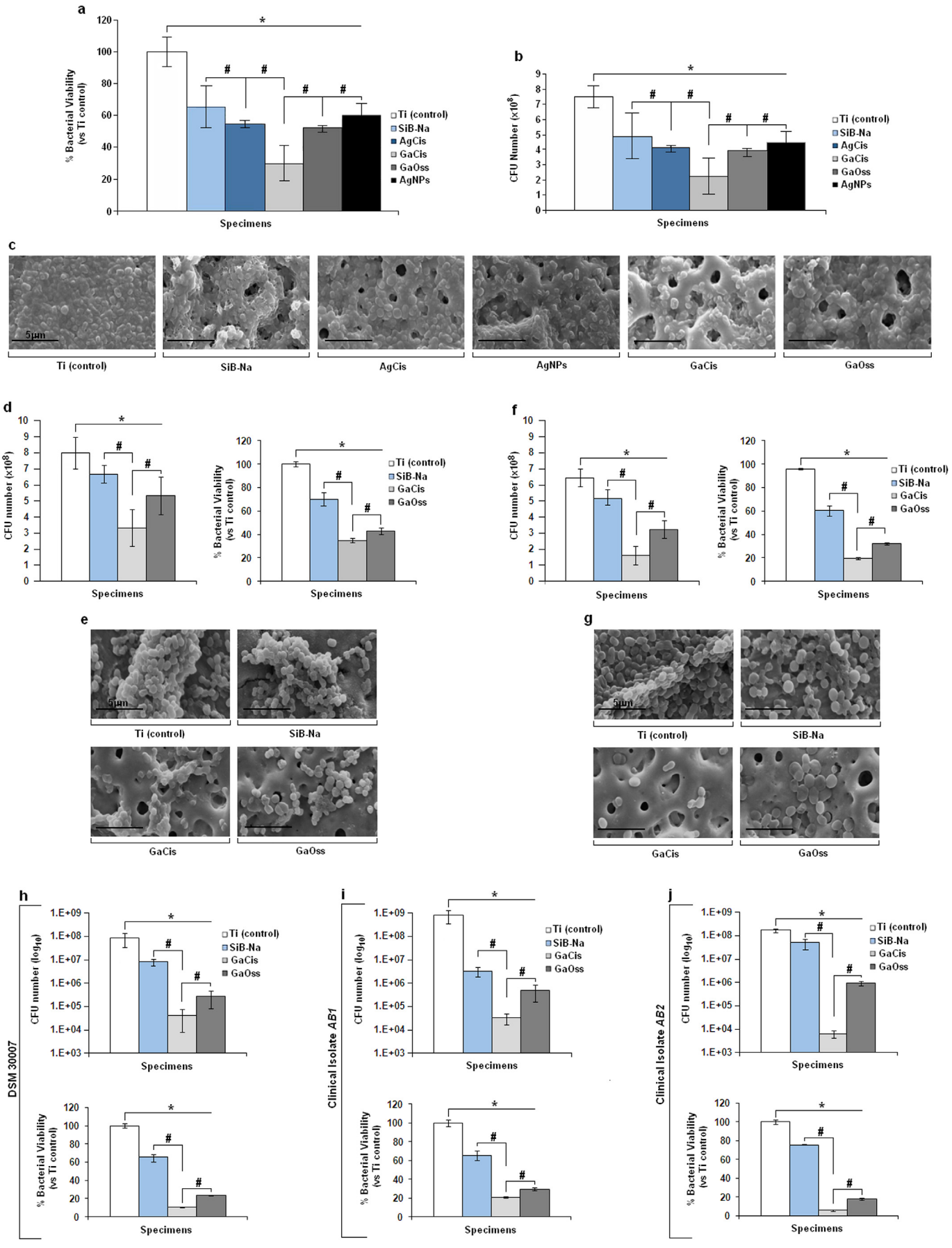
a
% Bacterial Viability (vs Ti control)
Specimens
Ti (control)
SiB-Na
AgCis
GaCis
GaOss
AgNPs
b
CFU Number (x10^8)
Specimens
Ti (control)
SiB-Na
AgCis
GaCis
GaOss
AgNPs
c
5μm
Ti (control)
SiB-Na
AgCis
AgNPs
GaCis
GaOss
d
CFU number (x10^8)
Specimens
% Bacterial Viability (vs Ti control)
Specimens
Ti (control)
SiB-Na
GaCis
GaOss
f
CFU number (x10^8)
Specimens
% Bacterial Viability (vs Ti control)
Specimens
Ti (control)
SiB-Na
GaCis
GaOss
e
5μm
Ti (control)
SiB-Na
GaCis
GaOss
g
5μm
Ti (control)
SiB-Na
GaCis
GaOss
h
DSM 30007
CFU number (log10)
Specimens
% Bacterial Viability (vs Ti control)
Specimens
Ti (control)
SiB-Na
GaCis
GaOss
i
Clinical Isolate AB1
CFU number (log10)
Specimens
% Bacterial Viability (vs Ti control)
Specimens
Ti (control)
SiB-Na
GaCis
GaOss
j
Clinical Isolate AB2
CFU number (log10)
Specimens
% Bacterial Viability (vs Ti control)
Specimens
Ti (control)
SiB-Na
GaCis
GaOss

from GaOss ($p < 0.05$, indicated by #). The XTT results were confirmed by the CFUs count. GaCis gave the lowest number of colonies: approx. one third of those on untreated controls, a difference that was significant in comparison with all other surfaces ($p < 0.05$, Fig. 7b, indicated by #). GaOss reduced CFUs to approx. one half of the control value, while silver reduced them by 1.6 times (both AgCis and AgNPs). Lastly, SEM observations (Fig. 7c) provided visual evidence that gallium treated surfaces were less colonized than either controls or silver treated surfaces, preventing the formation of complex 3-dimensional biofilm structures; in particular, GaCis showed an overall presence of single colonies, with some areas still uncontaminated.

These data suggested that gallium treatment provides higher efficacy in comparison with silver; antibacterial activity studies on GaCis and GaOss were thus extended to include two *A. baumanni* clinical isolates (*AB1* and *AB2*). The results are reported in Fig. 7 d–g, and confirm findings obtained with the commercial strain DSM 30007. In fact, *AB1* CFUs number (Fig. 7d, left panel) were significantly reduced by all the treatments respect to untreated controls ($p < 0.05$, indicated by *): in particular they were diminished of about 2.3 times by GaCis, while were decreased by SiB–Na and GaOss of about 1.2 and 1.4 times respectively. GaCis significantly differed also respect to SiB–Na and GaOss ($p < 0.05$, indicated by #). XTT analysis (Fig. 7d, right panel) showed similar trends: GaCis reduced bacterial viability by about 61 (±2) %, while SiB–Na and GaOss reduced it by 30 (±10) and 53 (±5) %, respectively. GaCis differed significantly from SiB–Na and GaOss ($p < 0.05$, indicated by #), while all treatments differed significantly from untreated controls ($p < 0.05$, indicated by *). SEM images (Fig. 7e) confirmed the metabolic observations visually, as the CaCis surfaces were clearly less contaminated than any of the others.

Results for the second clinical isolate, *AB2*, were very similar to those of *AB1* (Fig. 7f–g): although all doped surfaces were significantly different from untreated controls, in terms of both CFUs (Fig. 7f, left panel, $p < 0.05$ indicated by *) and XTT analysis (Fig. 7f, right panel, $p < 0.05$ indicated by *), GaCis was significant in comparison with GaOss and SiB–Na too ($p < 0.05$ indicated by #). Results were more marked than those obtained with *AB1*, the number of bacteria being reduced by about 3.6 times, and the viability by 80 (±3) %, compared with untreated controls. GaOss and SiB–Na were only reduced by 1.8–1.2 times, and by 66 (±6) − 38 (±5) %, respectively. Lastly, the SEM images (Fig. 7g) also showed that the CaCis surfaces were less contaminated than any of the others, confirming observations with *AB1*.

All the above results were obtained by cultivating bacteria with LB medium; this is a source of iron that competes for gallium in exerting antibacterial activity. Therefore, to clarify the activity of gallium in greater depth, all three *A. baumannii* strains (DSM 30007-*AB1*-*AB2*) were cultivated in an iron-chelated medium (MM9). The results are given in Fig. 7 h–j. In general, trends were comparable to those obtained with the LB medium; AgCis was the most active surface treatment in terms of bacterial inhibition, with values of CFUs and XTT differing significantly from those of untreated controls, SiB–Na, and GaOss. In detail, for the DSM 30007 strain (Fig. 7h) AgCis determined a reduction of about 3.2 logarithms (log) in CFUs (Fig. 7h, upper panel) and about 90 (±2)% for bacteria viability (Fig. 7h, lower panel) in comparison with untreated controls. GaOss also produced a significant inhibition (2.5 log and 77 ± 3%) in comparison with untreated controls, while the results for SiB–Na were very similar to those obtained with the LB medium (as expected, because this surface is gallium free). All treatments differed significantly from untreated controls ($p < 0.05$ indicated by *); GaCis also differed significantly from SiB–Na and GaOss ($p < 0.05$ indicated by #).

Clinical isolates were also more sensitive to gallium when cultivated in an iron-chelated medium. *AB1* colony numbers (Fig. 7i, upper panel) were reduced by about 4.2 log by GaCis, while viability (Fig. 7i, lower panel) was reduced by about 80 (±3) %. All results were significantly different from untreated controls ($p < 0.05$, indicated by *) and other treatments ($p < 0.05$, indicated by #). GaOss was effective (about 3 log for CFUs and 70 ± 6% viability reduction) and significantly different from untreated controls, while AB1 was mildly sensitive also to SiB–Na surfaces (about 2.3 log and 35 ± 5% reduction). All treatments differed significantly from untreated controls ($p < 0.05$ indicated by *) and GaCis differed significantly from SiB–Na and GaOss ($p < 0.05$ indicated by #).

Lastly, the strongest antibacterial effect was achieved with the *AB2* isolate cultivated in the MM9 medium (Fig. 7j). GaCis specimens showed a 4.6 log reduction of CFUs number (Fig. 7j, upper panel) and a 92 (±3) % viability reduction (Fig. 7j, lower panel), which differed significantly from controls ($p < 0.05$, indicated by *) and other treatments ($p < 0.05$, indicated by #). GaOss reduced bacterial numbers by about log 2.2, and viability by 78 (±2) %, while the AB2 strain was less sensitive to SiB–Na, which induced a reduction of about 1 log and 22 (±5) % in CFUs and viability. All treatments differed significantly from untreated controls ($p < 0.05$ indicated by *) and GaCis differed significantly from SiB–Na and GaOss ($p < 0.05$ indicated by #).

4. Discussion

The study examined the morphological, physico-chemical, biological, and antibacterial properties of some innovative biomimetic antibacterial silver and gallium surface modification treatments for titanium implants, in order to determine their anti-bacterial effectiveness toward the emergent MDR *A. Baumannii*. This was represented by the DSM 30007 strain and by two different clinical isolates, chosen because of the differing antimicrobial responses among commercial and wild-type strains.

Contact angle measurements showed all ASD treatments to be highly hydrophilic compared to untreated titanium. This effect was not related to the ASD surface roughness, since the Ra value was similar to that of the Ti surface (Fig. 1b); it could therefore be associated to the modified chemical composition of the ASD titanium oxide layer. Although all ASD surfaces doped with Ag or Ga

Fig. 7. a–j. *In vitro* bactericide activity. Biomimetic SiB–Na, silver (AgCis-AgNPs) and gallium (GaCis and GaOss) treatments determined a decrease in bacteria viability (a) and CFUs number (b) in comparison with control ($p < 0.05$, indicated by *) for DSM 30007 strain cultivated in LB medium. Moreover, the activity of GaCis was statistically significantly different from the other treated specimens ($p < 0.05$, indicated by #); SEM analysis (c) confirmed that GaCis specimens surfaces were the least colonized. Gallium antibacterial activity was confirmed by treating the clinical isolates *AB1* (d–e) and *AB2* (f–g) cultivated in LB medium. All the treatments were significant towards untreated control ($p < 0.05$, indicated by *), but GaCis was significant also in comparison with SiB–Na and GaOss ($p < 0.05$, indicated by #) for both *AB1* and *AB2* CFUs count (d and f respectively, right panels) and bacterial viability evaluation (d and f respectively, left panels). SEM images confirmed metabolic analysis by showing GaCis surfaces as the less contaminated ones for both *AB1* (e) and *AB2* (g) clinical isolates. Finally, when all the strains were cultivated in the iron-chelated MM9 medium, gallium inhibition was even higher if compared to LB medium assays (h–i–j). In fact, the CFUs count reported a decrease from about 3.2 to 4.6 logs for GaCis specimens that was always significant towards other treatments (h–i–j, upper panels, $p < 0.05$, indicated by #); also viability was largely lowered by GaCis (90 ± 2, 80 ± 3, 92 ± 3% for DSM 30007, *AB1* and *AB2* respectively) with significant values in comparison with other treatment (h–i–j, lower panels, $p < 0.05$, indicated by #). Doped surfaces were all significant in comparison with untreated controls (h–i–j, lower and upper panels, $p < 0.05$, indicated by *). For SEM images bar scale = 5 μm; magnification = 7500×.

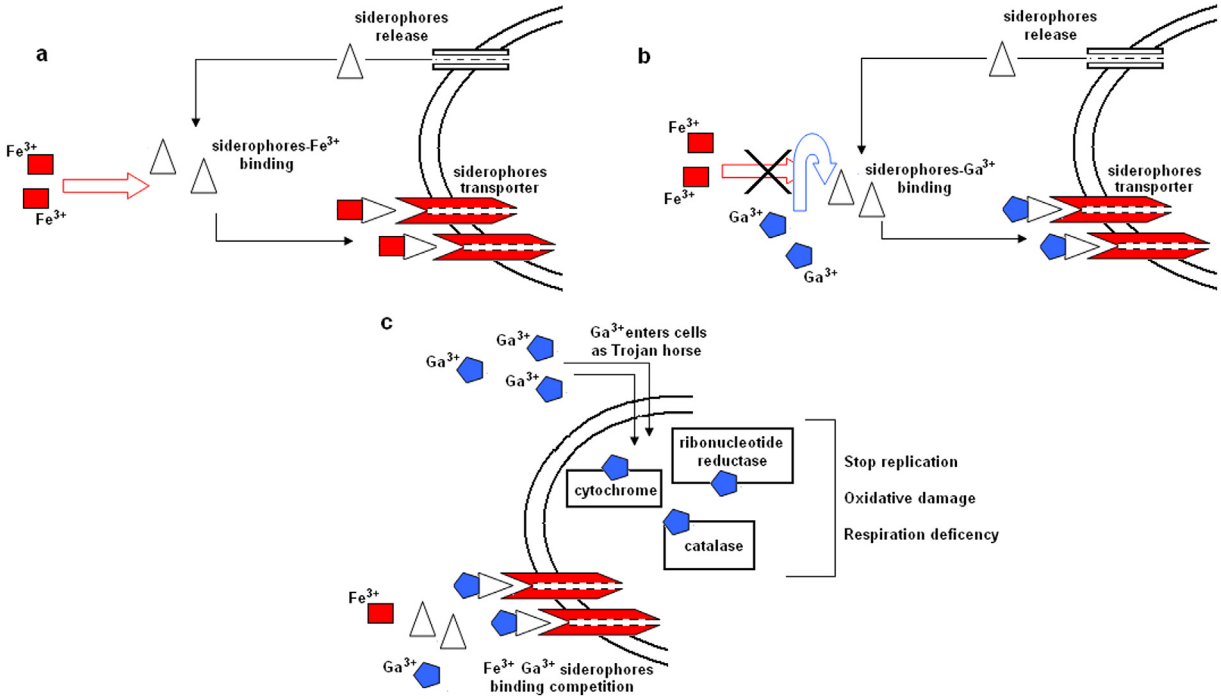

Fig. 8. Schematic representation of the gallium "Trojan horse" mechanism. In bacterial metabolism, the role of Fe^{3+} ions is crucial, and is mediated by intra-membrane transport via siderophores (a); gallium ions (Ga^{3+}) can effectively compete with Fe^{3+} for binding to siderophores (b), thus interrupting crucial Fe-dependent metabolic pathways in the bacterium. Moreover, Ga^{3+} can act intracellularly affecting iron homeostasis leading to different pathways damage (c).

were highly hydrophilic, it was unclear whether the difference in static contact angle between those surfaces and the SiB–Na control was caused by the presence of the antibacterial agents or by other factors (chelating agents, different treatment parameters). Nevertheless, the greater hydrophilicity of the control (SiB–Na) may probably be ascribed to the final NaOH alkali etching [12].

The chemical composition of the outer few nanometers of the different coatings tested by XPS analysis was very uniform, as expected of this electrochemical technique [29]. No silicon or phosphorous was present on the surface of the SiB–Na samples, these elements probably being removed by the alkali etching treatment. The sampling depth in the XPS and the EDS techniques is different, and the apparent discrepancies in the results might indicate that the surface composition differs from that of the deeper layers. For example, in the samples arising from SiB treatment, phosphorus was not detected by XPS analysis, whereas it was found by EDS analysis.

Surface enrichment with Ca, P and Si species plays a fundamental role in enhancing the mineralization process of titanium implantable devices [12,30]. Thus the Ca/P signal area ratios were calculated for those specimens in which both Ca2p and P2p signals were recorded. In particular, $Ca(H_2PO_4)_2$ and $CaHPO_4$ showed Ca/P ratios of 0.5 and 1, respectively, while other apatite-like species (i.e., $Ca_3(PO_4)_2$, hydroxyapatite: $Ca_5(PO_4)_3(OH)$, apatite: $Ca_{10}(PO_4)_6(OH)_2$, or octacalcium-phosphate: $Ca_8H_2(PO_4)_6\cdot 5H_2O$) had Ca/P ratios $\geq$1.5. It thus appears that, on the SiB, AgNPs, AgCis and GaCis surfaces, $Ca(H_2PO_4)_2$ and $CaHPO_4$ may coexist, the latter predominating (i.e. Ca/P = 0.8, 0.93, 1.06 and 0.96, in SiB, AgNPs, AgCis and GaCis specimens, respectively).

The absence of calcium in the GaOss specimens is probably due to a set of factors: (i) the different voltage applied creates dissimilar pore morphology; (ii) the presence of oxalic acid, as chelating agent for gallium nitrate, might have a competitive embedding effect in the titanium oxide layer at the anode between calcium and silicon (markedly more silicon was found in GaOss than in GaCis specimens). In regard to the silver-based antibacterial treatments, XPS analysis detected more Ag in the AgCis than in the AgNPs specimens, as evidenced by the Ag/Ti ratios. As far as the chemical nature of silver in the analyzed treatments is concerned, the XPS Ag3d signals recorded do not distinguish between Ag(I) and Ag(0), due to their similar BE values. The relevant Ag MNN Auger signals could provide this information, but the intensity of these signals was below the detection limit of the technique, since the amount of silver present in both AgCis and AgNPs was very low. Conversely, for the gallium-based treatments, XPS revealed a slightly larger amount of gallium on the GaOss than on the GaCis surface, as evidenced by the Ga/Ti ratios. The experimental BEs associated to Ga2p are typical of gallium (III) compounds [31]. The capability of titanium to embed different cations in its crystallographic structure is well documented [32]. The presence of Ti doublets, at binding energies higher than titanium oxides, might be ascribable to titanates (Fig. 3b–e); although detected on all the surfaces investigated, these species were present in larger amounts after SiB–Na treatment than after SiB treatment. On the silver-based specimens, the TiO_2/titanates ratio was very similar to that of the SiB specimens, whereas on gallium-based specimens, surface titanates predominated (Fig. 3f). It is worth noting that the predominant surface occurrence of titanates on the gallium-based antibacterial specimens might play an interesting role, positively affecting the mineralization process, as well as osteoblastic proliferation and differentiation, as has been reported for calcium and sodium titanates [33–35].

Analysis of the titanium oxide cross-sections showed that the thickness was constant along the line of analysis, with no significant discontinuities or irregularities. AgCis and GaCis, with different antibacterial agents but the same chelating agent (cistein), showed similar morphology and thickness; thus the markedly reduced thickness observed for GaOss might reasonably be

ascribed to the presence of oxalic acid in the electrolytic solution, which radically modifies ion transport and film growth conditions. Considering that, for a given deposition system, film thickness may affect adhesion to the substrate [29], very thick ASD coatings are potentially more susceptible to breakage and delamination.

With the ASD technique, thick and hard ceramic coatings can be deposited on titanium [36,37]. Vickers micro-hardness measurements showed that the ASD treatments tested here increased the surface hardness of titanium 2–5 times. Nevertheless, no particular susceptibility to brittle fracture was evidenced for any of the ASD treatments tested (images not shown). The elastic modulus of the ASD titanium oxide layers was found to be lower than untreated titanium for all ASD treatments, with the control SiB–Na possessing the lowest elastic modulus. As has been reported [38], the porous structure of the ASD coating appears to contribute to decreasing the elastic modulus in comparison to untreated titanium. Moreover, it has been suggested [39] that soft calcium phosphate agglomerates, produced inside the layer during anodization, may contribute to decreasing the elastic modulus. A low elastic modulus, closer to that of bone tissues, which ranges from 10 to 20 GPa [40], may confer some advantages on implanted devices, allowing a more physiological load transfer between implant and bone, and also stimulating bone tissue growth [39]. It is interesting that the ASD treatments tested here had a lower elastic modulus than other ASD treatments produced using different electrolytic solutions.

Delamination did not occur on any of the ASD treatments at the bending test. The cracks observed on AgNPs surface were mainly around the pores, while in AgCis and GaCis, cracks mainly ran across the pores. GaCis had fewer cracks than AgCis or AgNPs, while no cracks were observed on GaOss. This latter observation might reasonably be attributed to the reduced thickness of the titanium oxide layer improving its mechanical performance, and to the compactness of the anodic oxide growth.

In all cases, the scratch test findings indicated high shear stress values, including in the case of AgNPs, which had the lowest critical load values. It is interesting that the critical shear stress of the ASD coating was five times the average load acting on the hip joint when walking (i.e. 35 MPa) [41] and almost one order of magnitude higher than the value reportedly necessary for orthopedic prostheses (>22 MPa) [42].

The release test of the antibacterial agents from the ASD treated surface, performed in 5 mL of D-PBS calcium-free solution, provided the results shown in Fig. 5. Silver was released gradually from the AgNPs coating, after an initial burst. Although the total amount of silver on the AgCis surface was higher than that on AgNPs, as shown by XPS analysis, four times less silver was released from AgCis than from AgNPs. The gradual release of silver from AgNPs may be attributed to the oxidation mechanism of the silver nanoparticles in the ASD coating entering in contact to the water-based D-PBS solution, as has been hypothesized [43]. In general, Ag^{+} species show stronger antibacterial activity than metallic Ag (0). The ICP-OES results do not distinguish between Ag^{+} and zero-valent Ag (0) species in solution, and thus from these tests it was not possible to determine whether both species were present in the D-PBS solution. Although other studies cannot be compared directly to these tests, due to differences in experimental conditions, the concentration found here was considerably below the toxic silver concentration threshold for eukaryotic cell growth, which is reported to be 1–10 mg/L for silver ions and 10–100 mg/L for silver nanoparticles [43]. Additionally, the silver concentration effective against prokaryotic cells has already been shown to be 0.1 mg/L, which is quite close to the silver released from the present samples. The sample surface was 2.26 cm^2; maximum release was 52 μg/L and 180 μg/L, from AgCis and AgNPs, respectively.

Although the gallium content of GaCis was similar to that of GaOss, as the XPS data showed, the release kinetics of the two surfaces was completely different, gallium being released from the GaOss surface more than fifty times more abundantly quickly than from GaCis. The amount of calcium found in GaCis samples could explain the low gallium release from these systems, probably due to the interaction between gallium and CaP species [44,45]. Conversely, in the GaOss specimens, calcium was not detected, and gallium loosely bound to the surface could explain the observed release behavior.

It should also be stressed, however, that in this preliminary study the release mechanism was determined in D-PBS solution, with stable and fixed pH, whereas release kinetics may differ at different pH values, or be influenced by different *in vivo* environmental factors, e.g. they might be related to inflammation or infections.

The human epithelial-like primary osteogenic sarcoma Saos2 cell line, used for the biological characterization, possesses some markers and a phenotype typical of primary human osteoblasts cultured on metallic surfaces [46,47]. The results of the *in vitro* indirect cytotoxicity assay showed no significant cytotoxic effect up to 21 days for Saos2 cultured in medium conditioned by the leachable products released from the test specimens; the presence of antibacterial agents did not affect the cells' metabolic activity vs. controls.

The cells were found to adhere more closely to the antibacterial surfaces than they did to simple titanium; their morphology remained unaltered, and their viability good. It might be hypothesized that the elevated hydrophilicity and surface energy provided by the ASD coating favor osteoblastic cell adhesion; additionally, the porous morphology offers preferential sites for cell attachment and spreading, versus untreated titanium; this confirms what has been reported in other studies [48–54].

It is interesting that, especially on ASD coatings, there were many cells in the replication phase, together with cell-to-cell interactions, well defined focal points, and stress fibers [28] on the actin filaments, confirming rapid cellular spreading. Saos2 cells metabolic activity increased from day 1–21 of contact with the test surfaces.

In general, there was no marked difference in cell viability between the different coatings tested; however, a direct cytotoxic effect caused by the antibacterial element present on the sample surfaces could be ruled out. ALP synthesis, which is one of the most important markers of osteogenic activity and new bone formation, was significantly higher in Saos2 cells cultured with ASD samples than with untreated titanium controls. The ASD coatings stimulated Saos2 osteogenic activity; this activity was comparable between antibacterial coated samples and SiB–Na controls, despite the presence of antibacterial agents. Interestingly, GaOss treatment showed significantly higher ALP activity than the other ASD antibacterial treatments, being better than the optimum control SiB–Na. Thus not only did the presence of gallium as antibacterial agent not interfere with ALP production, it apparently determined a stimulating effect on osteoblastic activity toward new bone matrix formation. This effect was more evident in the case of GaOss treatment, because of the presence of gallium, and gallium release from the surface was higher than for the GaCis treatment. The high level of ALP for the gallium-based treatments was in line with some *in vivo* studies, in which the presence of gallium was associated with enhanced bone formation and elevated ALP expression.

Many factors may affect the initial attachment of microorganisms to substrata, and their subsequent retention or removal/detachment, including the physico-chemical nature and location of the substratum, the type of organic material and microorganisms potentially fouling the surface, and the nature of the interface [55].

To better evaluate the antimicrobial activity of surfaces doped with gallium, whose efficacy is suggested to be mainly related to competition with iron (Fig. 8), and to mimic human plasma, whose free iron concentration is about 10^{-8} M, experiments were done using "iron-chelated" minimal medium (MM9), in addition to conventional use of commercial LB media.

As expected, in MM9 the antibacterial activity of gallium against all three *A. baumannii* strains tested was found to be amplified compared to that in LB medium, especially for GaCis, suggesting that the low and gradual release of gallium from the GaCis specimens, as observed in the D-PBS release test, could efficaciously discourage the colonization and proliferation of the tested bacteria on these titanium surfaces (Fig. 7). At the tests to evaluate the antibacterial activity of the coatings, specimens treated with GaCis in particular showed good inhibition of biofilm formation by all three strains of *A. baumannii,* a very powerful Gram-negative biofilm-producer; this bacterium was used as test microorganism since it is an emerging operating-theatre pathogen, often giving rise to dangerous multidrug resistant infections with serious clinical implications [56]. As schematized in Fig. 8, gallium is metabolically very similar to Fe^{3+}, acting as an iron substitute in several biological pathways. Thanks to its chemical similarity to Fe^{3+} in terms of charge, ionic radius, electronic configuration, and coordination number, gallium can substitute iron in siderophore-dependent biological systems; this capability underlies its antibacterial action. Since Ga^{3+} cannot be reduced under the same conditions as Fe^{3+}, sequential redox reactions critical for the biological functions of Fe^{3+} are impaired when iron is replaced: gallium thus inhibits Fe^{3+} by a "Trojan horse" strategy [57–59].

SiB–Na treatment also showed more intense antibacterial activity against *A. baumannii* biofilm than untreated titanium. The presence of anatase might confer antibacterial activity to all the ASD coatings; this effect is enhanced in the case of GaOss and GaCis, thanks to the presence of gallium. The high hydrophilicity and surface energy of the ASD surfaces might also play a beneficial role, reducing biofilm cell attachment to the substrate, and limiting subsequent proliferation.

Recent findings suggest that gallium-iron competition can lead to a cellular iron deficiency status, thus inducing the expression of pathogenic factors able to increase the virulence at least of *P. aeruginosa* [58]. It has also been demonstrated that iron deficiency alone can promote the production of biofilm by *P. aeruginosa* and *A. baumannii* [59].

In the model employed here, Ga competition with Fe for binding to siderophores did not increase the virulence of *A. baumannii*. It might be speculated that, in this system, the results for GaCis were better than those for GaOss since Ga release, as observed in the release test, was lower, but not low enough to cause complete iron deficiency, which can enhance virulence [59]. To summarize, the antibacterial ASD coatings were characterized by uniform and reproducible chemico-physical properties appropriate to favor osteoblast attachment and proliferation. In particular, the treated surfaces provided attractive platforms for osteoblast differentiation toward the production of new bone tissue. Next to the optimum control (SiB–Na), the GaOss-based treatment was that which best promoted osteoblast adhesion, spreading, colonization, and proliferation, also stimulating the production of new bone tissue. The presence of antibacterial agents in the coatings, together with their release kinetics, conferred a marked ability to inhibit biofilm growth, in the present test conditions.

5. Conclusions

The emergence of MDR bacteria, and the reduced effectiveness of antibiotics, along with the increasing number of failures of arthroplasty and osteosynthesis due to implant-related infections of biomaterials, have generated increasing demand for different strategies to counteract infections.

This study demonstrated the possibility of successfully using Anodic Spark Deposition (ASD) to develop biomimetic treatments on titanium substrates, as a valid antibacterial strategy, offering the advantage of locally-controlled delivery of gallium or silver ions, with no danger of developing new bacterial resistance, while maintaining high osteointegrative potential.

These substrates were found to possess properties appropriate to favor the production of new bone tissue, with results comparable to the SiB–Na control already in clinical use. Moreover, the antibacterial agents embedded in the ASD-modified titanium oxide, released over a long period of time, gave the treated titanium bacteriostatic and bactericidal properties, in particular strongly inhibiting the formation of biofilm by *A. baumannii,* an emergent opportunistic bacterial strain frequently responsible for titanium-implant associated infections. The surface coatings also showed good hardness, film adhesion and cohesion, and no delamination even under bending. The antibacterial coatings can readily be scaled up to industrial level, being produced by a rapid single-step ASD process, similar to the SiB–Na treatment, which has already been tested clinically. Furthermore, since gallium is already on the US FDA approved list, it may be used *in vivo*.

In the light of these considerations, it may be concluded that the proposed ASD treatments possess all the credentials for use as adaptable preventive and therapeutic antibacterial agents, and are promising candidate techniques, offering antibacterial capabilities together with high osteointegrative properties, thus being appropriate for dental and orthopedic applications. Among the treatments tested, the gallium-based treatments, in particular GaOss and GaCis, showed peculiar and interesting properties, and are thus the best candidates for future studies.

This work clearly shows, for the first time to the authors' knowledge, the potential use of the Anodic Spark Deposition (ASD) technique for doping titanium surfaces with gallium or silver ions to stimulate osteointegration, thanks to its efficacy in blocking osteoclast resorption, combined with its marked antibacterial activity against the test bacterium *A. baumannii*.

As further confirmation of these data, the antibacterial properties of gallium should be evaluated, in combination or not with silver, on other hospital MDR and biofilm former clinical isolates, mainly those belonging to the "ESKAPE" pathogens.

Funding

B. A. was supported by "Fondazione Cariplo 2013" (prot. 2013-0954); A. C. and B. A. were supported by PRIN 2010–2011 (PRIN 20102ZLNJ5_006), financed by the Ministry of Education, University and Research (M.I.U.R.), Rome, Italy. L.V. would like to acknowledge financial support from MIUR, PRIN 2010-11 (prot. 2010FPTBSH_009). The providers of funds played no role in study design, data collection and analysis, decision to publish, or preparation of the manuscript.

Acknowledgments

The authors thank Eurocoating S. p. A. We are grateful to P. Vaghi (Centro Grandi Strumenti, University of Pavia) and D. Picenoni (Politecnico di Milano, Milano, Italy) for technical assistance in the CLSM and SEM studies, respectively.

Finally, authors would like to thank Frances Cooper for language revision.

References

[1] I. Armentano, C.R. Arciola, E. Fortunati, D. Ferrari, S. Mattioli, C.F. Amoroso, et al., The interaction of bacteria with engineered nanostructure polymeric materials: a review, Sci. World J. 2014 (2014) 410423, http://dx.doi.org/10.1155/2014/410423.

[2] M. Bassetti, F. Ginocchio, M. Mikulska, New treatment options against gram-negative organisms, Crit. Care 15 (2011) 215, http://dx.doi.org/10.1186/cc9997.

[3] A. Howard, M. O'Donoghue, A. Feeney, R.D. Sleator, Acinetobacter baumannii: an emerging opportunistic pathogen, Virulence 3 (2012) 243–250, http://dx.doi.org/10.4161/viru.19700.

[4] S. Bayuga, C. Zeana, J. Sahni, P. Della-Latta, W. el-Sadr, E. Larson, Prevalence and antimicrobial patterns of Acinetobacter baumannii on hands and nares of hospital personnel and patients: the iceberg phenomenon again, Heart Lung 31 (2002) 382–390, http://dx.doi.org/10.1067/mhl.2002.126103.

[5] P.E. Fournier, D. Vallenet, V. Barbe, S. Audic, H. Ogata, L. Poirel, et al., Comparative genomics of multidrug resistance in Acinetobacter baumannii, PLoS Genet. 2 (1) (2006) e7, http://dx.doi.org/10.1371/journal.pgen.0020007.

[6] N.M. Anstey, B.J. Currie, M. Hassell, D. Palmer, B. Dwyer, H. Seifert, Community-acquired bacteremic Acinetobacter pneumonia in tropical Australia is caused by diverse strains of Acinetobacter baumannii, with carriage in the throat in at-risk groups, J. Clin. Microbiol. 40 (2002) 685–686, http://dx.doi.org/10.1128/JCM.40.2.685-686.2002.

[7] F. Perez, A.M. Hujer, K.M. Hujer, B.K. Decker, P.N. Rather, R.A. Bonomo, Global challenge of multidrug-resistant Acinetobacter baumannii, Antimicrob. Agents Chemother. 51 (10) (2007) 3471–3484, http://dx.doi.org/10.1128/AAC.01464-06.

[8] M. Geetha, A.K. Singh, R. Asokamani, A.K. Gogia, Ti based biomaterials, the ultimate choice for orthopaedic implants. A review, Prog. Mater. Sci. 54 (2009) 397e425, http://dx.doi.org/10.1016/j.pmatsci.2008.06.004.

[9] L. Rimondini, C. Della Valle, A. Cochis, B. Azzimonti, R. Chiesa, The biofilm formation onto implants and prosthetic materials may be contrasted using Gallium (3^{+}), Key Eng. Mater. 587 (2014) 315–320, http://dx.doi.org/10.4028/www.scientific.net/KEM.587.315.

[10] Z. Lingzhou, K.C. Paul, Z. Yumei, W. Zhifen, Antibacterial Coatings on Titanium Implants, J. Biomed. Mater. Res. B Appl. Biomater. 91 (2009) 470–480.

[11] C.R. Chitambar, Gallium-containing anticancer compounds, Future Med. Chem. 4 (10) (2012) 1257–1272, http://dx.doi.org/10.4155/fmc.12.69.

[12] C. Della Valle, G. Rondelli, A. Cigada, A.E. Bianchi, R. Chiesa, A novel silicon-based electrochemical treatment to improve osteointegration of titanium implants, J. Appl. Biomater. Funct. Mater. 11 (2013) 106–116, http://dx.doi.org/10.5301/JABFM.2012.9419.

[13] M.J. Coathup, S. Samizadeh, Y.S. Fang, T. Buckland, K.A. Hing, G. Blunn, The Osteoinductivity of silicate-substituted Calcium Phosphate, J. Bone Jt. Surg. Am. 93 (2011) 2219–2226, http://dx.doi.org/10.2106/JBJS.I.01623.

[14] A. Cochis, B. Azzimonti, C. Della Valle, R. Chiesa, C.R. Arciola, L. Rimondini, Biofilm formation on titanium implants counteracted by grafting gallium and silver ions, J. Biomed. Mater. Res. A 103 (2015) 1176–1187, http://dx.doi.org/10.1002/jbm.a.35270.

[15] D. Briggs, M.P. Seah, Practical Surface Analysis, Auger and X-ray Photoelectron Spectroscopy, Wiley, Chichester, UK, 1990.

[16] E. De Giglio, S. Cometa, M.A. Ricci, D. Cafagna, A.M. Savino, L. Sabbatini, et al., Ciprofloxacin-modified electrosynthesized hydrogel coatings to prevent titanium-implant-associated infections, Acta Biomater. 7 (2011) 882–891, http://dx.doi.org/10.1016/j.actbio.2010.07.030.

[17] G.B. De Souza, G.G. de Lima, N.K. Kuromoto, P. Soares, C.M. Lepienski, C.E. Foerster, et al., Tribo-mechanical characterization of rough, porous and bioactive Ti anodic layers, J. Mech. Behav. Biomed. Mater. 4 (2011) 796–806, http://dx.doi.org/10.1016/j.jmbbm.2010.09.012.

[18] M.H. Blees, G.B. Winkelman, A.R. Balkenende, J.M.J. den Toonder, The effect of friction on scratch adhesion testing: application to a sol-gel coating on polypropylene, Thin Solid Films 359 (2000) 1–13, http://dx.doi.org/10.1016/S0040-6090(99)00729-4.

[19] J. Sambrook, D.W. Russell, Molecular Cloning: a Laboratory Manual, third ed., Cold Spring Harbor Laboratory Press, USA, 2001.

[20] J. Li, P. Han, W. Ji, Y. Song, S. Zhang, Y. Chen, et al., The in vitro indirect cytotoxicity test and in vivo interface bioactivity evaluation of biodegradable FHA coated Mg–Zn alloys, Mater. Sci. Eng. B 176 (2011) 1785–1788, http://dx.doi.org/10.1016/j.mseb.2011.05.029.

[21] M.S. Sbarra, C.R. Arciola, A. Di Poto, E. Saino, H. Rohde, P. Speziale, et al., The photodynamic effect of tetra-substituted N-methyl-pyridyl-porphine combined with the action of vancomycin or host defense mechanisms disrupts Staphylococcus epidermidis biofilms, Int. J. Artif. Organs 32 (2009) 574–583.

[22] H. Nailis, T. Coenye, F. Van Nieuwerburgh, D. Deforce, H.J. Nelis, Development and evaluation of different normalization strategies for gene expression in Candida albicans biofilms by real-time PCR, BMC Mol. Biol. 7 (2006) 25–36, http://dx.doi.org/10.1186/1471-2199-7-25.

[23] K. Honraet, E. Goetghebeurb, H.J. Nelis, Comparison of three assays for the quantification of Candida biomass in suspension and CDC reactor grown biofilms, J. Microbiol. Methods 63 (2005) 287–295, http://dx.doi.org/10.1016/j.mimet.2005.03.014.

[24] D.M. Kuhn, M. Balkis, J. Chandra, P.K. Mukherjee, M.A. Ghannoum, Uses and limitations of the XTT assay in studies of Candida growth and metabolism, J. Clin. Microbiol. 41 (2003) 506–508, http://dx.doi.org/10.1128/JCM.41.

[25] F. Rivardo, R.J. Turner, G. Allegrone, H. Ceri, M.G. Martinotti, Anti - adhesion activity of two biosurfactants produced by Bacillus spp. prevents biofilm formation of human bacterial pathogens, Appl. Microb. Biotechnol. 83 (2009) 541–553, http://dx.doi.org/10.1007/s00253-009-1987-7.

[26] J.J. Harrison, H. Ceri, J. Yerly, C.A. Stremick, Y. Hu, R. Martinuzzi, et al., The use of microscopy and three-dimensional visualization to evaluate the structure of microbial films cultivated in the Calgary biofilm device, Biol. Proced. Online 8 (2006) 194–215, http://dx.doi.org/10.1251/bpo127.

[27] E. Brambilla, A. Ionescu, M. Gagliani, A. Cochis, C.R. Arciola, L. Rimondini, Biofilm formation on composite resins for dental restorations: an in situ study on the effect of chlorhexidine mouthrinses, Int. J. Artif. Organs 35 (2012) 792–799, http://dx.doi.org/10.5301/ijao.5000165.

[28] C. Li, S. Gao, T. Terashita, T. Shimokawa, H. Kawahara, S. Matsuda, et al., In vitro assay fro adhesion and migration of osteoblastic cells (Saos2) on titanium surfaces, Cell Tissue Res. 324 (2006) 369–375, http://dx.doi.org/10.1007/s00441-005-0153-5.

[29] R. Chiesa, E. Sandrini, M. Santin, G. Rondelli, A. Cigada, Osteointegration of titanium and its alloys by anodic spark deposition and other electrochemical techniques: a review, J. Appl. Biomater. Biomech. 1 (2003) 91–107 (Doi not available).

[30] X. Liu, P.K. Chu, C. Ding, Surface modification of titanium, titanium alloys, and related materials for biomedical applications, Mater. Sci. Eng. 47 (2004) 49–121, http://dx.doi.org/10.1016/j.mser.2004.11.00.

[31] NIST X-ray Photoelectron Spectroscopy Database, Version 4.1, National Institute of Standards and Technology, Gaithersburg, 2012. http://srdata.nist.gov/xps/.

[32] V.V. Atuchin, V.G. Kesler, N.V. Pervukhina, Z. Zhang, Ti 2p and O 1s core levels and chemical bonding in titanium bearing oxides, J. Electron Spectrosc. Relat. Phenom. 152 (2006) 18–24, http://dx.doi.org/10.1016/j.elspec.2006.02.004.

[33] S.S. Hakki, P. Korkusuz, N. Purali, F. Korkusuz, B.S. Bozkurt, E.E. Hakki, et al., Periodontal ligament cell behavior on different titanium surfaces, Acta Odontol. Scand. 71 (2013) 906–916, http://dx.doi.org/10.3109/00016357.2012.734417.

[34] P. Korkusuz, S.S. Hakkı, N. Puralı, I. Görür, E. Önder, R. Nohutçu, et al., Interaction of MC3T3-E1 cells with titanium implants, Jt. Dis. Rel Surg. 19 (2008) 84–90.

[35] J.B. Nebe, L. Müller, F. Lüthen, A. Ewald, C. Bergemann, E. Conforto, et al., Osteoblast response to biomimetically altered titanium surfaces, Acta Biomater. 4 (2008) 1985–1995, http://dx.doi.org/10.1016/j.actbio.2008.05.028. Doi not available.

[36] W. Xue, C. Wang, R. Chen, Z. Deng, Structure and properties characterization of ceramic coatings produced on Ti–6Al–4V alloy by microarc oxidation in aluminate solution, Mater. Lett. 52 (2002) 435–441, http://dx.doi.org/10.1016/S0167-577X(01)00440-2.

[37] W. Xue, Z. Deng, R. Chen, Z. Zhang, Microstructure and mechanical properties near the interface between microarc oxidation coating and aluminum alloy substrate, Surf. Eng. 16 (4) (2000) 344–348, http://dx.doi.org/10.1179/026708400101517242.

[38] B.D. Flinn, R.K. Bordia, A. Zimmermann, J. Rodel, Evolution of defect size and strength of porous alumina during sintering, J. Eur. Ceram. Soc. 20 (2000) 2561–2568, http://dx.doi.org/10.1016/S0955-2219(00)00133-3.

[39] G.B. de Souza, C.M. Lepienski, C.E. Foerster, N.K. Kuromoto, P. Soares, H. de Araújo Ponte, Nanomechanical and nanotribological properties of bioactive titanium surfaces prepared by alkali treatment, J. Mech. Behav. Biomed. Mater. 4 (2011) 756–765, http://dx.doi.org/10.1016/j.jmbbm.2010.07.005.

[40] J.Y. Rho, R.B. Ashman, C.H. Turner, Young's modulus of trabecular and cortical bone material: ultrasonic and microtensile measurements, J. Biomech. 26 (1993) 111–119, http://dx.doi.org/10.1016/0021-9290(93)90042-D.

[41] L.L. Zhang, H.J. Li, J.H. Lu, Li Kz, S. Coa, X.N. Zhao, et al., Surface characteristic and cell response of CVD SiC coating for carbon/carbon composites used for hip arthroplasty, Surf. Interface Anal. 44 (2012) 1319–1323, http://dx.doi.org/10.1002/sia.5021.

[42] A.V. Zavgorodniy, O. Berrero-Lopez, M. Hoffman, Mechanical stability of two step chemically deposited hydroxyapatite coating on Ti substrate: effects of various surface pretreatments, J. Biomed. Mater. Res. B Appl. Biomat. 99B (2011) 58–69, http://dx.doi.org/10.1002/jbm.b.31872.

[43] S. Chernousova, M. Epple, Silver as antibacterial agent: ion, nanoparticle, and metal, Angew. Chem. Int. Ed. Engl. 52 (2012) 1636–1653, http://dx.doi.org/10.1002/anie.201205923.

[44] L.R. Bernstein, Mechanisms of therapeutic activity for gallium, Pharmacol. Rev. 50 (1998) 665–682.

[45] S.P. Valappil, D. Ready, E.A. Abou Neel, D.M. Pickup, L.A. O'Dell, W. Chrzanowski, J. Pratten, R.J. Newport, M.E. Smith, M. Wilson, J.C. Knowles, Controlled delivery of antimicrobial gallium ions from phosphate-based glasses, Acta Biomater. 5 (2009) 1198–1210, http://dx.doi.org/10.1016/j.actbio.2008.09.019.

[46] L. Saldana, F. Bensiamar, A. Bore, N. Vilaboa, In search representative models of human bone-forming cells for cytocompatibility studies, Acta Biomater. 7 (2011) 4210–4221, http://dx.doi.org/10.1016/j.actbio.2011.07.019.

[47] L. Shapira, A. Halabi, Behavior of two osteoblast-like cell lines cultured on machined or rough titanium surfaces, Clin. Oral Impl. Res. 20 (2009) 50–55, http://dx.doi.org/10.1111/j.1600-0501.2008.01594.x.

[48] L. Le Guéhennec, A. Soueidan, P. Layrolle, Y. Amouriq, Surface treatments of titanium dental implants for rapid osseointegration, Dent. Mater. 23 (2007)

844–854, http://dx.doi.org/10.1016/j.dental.2006.06.025.
[49] K. Mustafa, A. Wennerberg, J. Wroblewski, K. Hultenby, B. Silva Lopez, et al., Determining optimal surface roughness of TiO2 blasted titanium implant material for attachment, proliferation and differentation of cells derived from human mandibular alveolar bone, Clin. Oral Implant Res. 12 (2001) 515–525, http://dx.doi.org/10.1034/j.1600-0501.2001.120513.x.
[50] M. Vandrovcova, J. Hanus, M. Drabik, O. Kylian, H. Biederman, V. Lisa, et al., Effect of different surface nanoroughness of titanium dioxide films on the growth of human osteoblast-like MG63 cells, J. Biomed. Mater. Res. A 100 (2012) 1016–1032, http://dx.doi.org/10.1002/jbm.a.34047.
[51] K.H. Frosch, F. Barvencik, V. Viereck, C.H. Lohmann, K. Dresing, J. Breme, et al., Growth behavior, matrix production, and gene expression of human osteoblasts in defined cylindrical titanium channels, J. Biomed. Mater. Res. A 68 (2004) 325–334, http://dx.doi.org/10.1002/jbm.a.20010.
[52] S.H. Oh, R.R. Finones, C. Daraio, L.H. Chen, S. Jin, Growth of nano-scale hydroxyapatite using chemically treated titanium oxide nanotubes, Biomaterials 26 (2005) 4938–4943, http://dx.doi.org/10.1016/j.biomaterials.2005.01.048.
[53] C. Aparicio, A. Padró, F.J. Gil, In vivo evaluation of microrough and bioactive titanium dental implants using histometry and pull-out tests, J. Mech. Behav. Biomed. Mater. 4 (2011) 1672–1682, http://dx.doi.org/10.1016/j.jmbbm.2011.05.005.
[54] B.H. Lee, J.K. Kim, Y.D. Kim, K. Choi, K.H. Lee, In vivo behavior and mechanical stability of surface modified titanium implants by plasma spray coating and chemical treatments, J. Biomed. Mater. Res. A 69 (2004) 279–285, http://dx.doi.org/10.1002/jbm.a.20126.
[55] J. Verran, K. Whitehead, Factors affecting microbial adhesion to stainless steel and other materials used in medical devices, Int. J. Artif. Organs 28 (2005) 1138–1145 (Doi not available).
[56] C.T. Selçuk, M. Durgun, B. Ozalp, A. Tekin, R. Tekin, C. Akçay, et al., Comparison of the antibacterial effect of silver sulfadiazine 1%, mupirocin 2%, Acticoat and octenidine dihydrochloride in a full-thickness rat burn model contaminated with multi drug resistant Acinetobacter baumannii, Burns 38 (2012) 1204–1209, http://dx.doi.org/10.1016/j.burns.2012.04.009.
[57] Y. Kaneko, M. Thoendel, O. Olakanmi, B.E. Britigan, P.K. Singh, The transition metal gallium disrupts Pseudomonas aeruginosa iron metabolism and has antimicrobial and antibiofilm activity, J. Clin. Investig. 117 (2007) 877–888, http://dx.doi.org/10.1172/JCI30783.
[58] R. Garcia-Contreras, B. Perez-Eretza, E. Lira-Silva, R. Jasso-Chavez, R. Coria-Jimenez, A. Rangel-Vega, T. Maeda, T.K. Wood, Gallium induces the production of virulence factors in Pseudomonas aeruginosa, Pathog. Dis. 70 (2014) 95–98, http://dx.doi.org/10.1111/2049-632X.12105.
[59] F. Modarresi, O. Azizi, M.R. Shakibaie, M. Motamedifar, E. Mosadegh, S. Mansouri, Iron limitation enhances acyl homoserine lactone (AHL) production and biofilm formation in clinical isolates of Acinetobacter baumannii, Virulence 6 (2015) 152–161, http://dx.doi.org/10.1080/21505594.2014.1003001.